CROATICA CHEMICA ACTA CCACAA **69** (3) 1069–1115 (1996)

ISSN-0011-1643
CCA–2363

Original Scientific paper

Diffraction Line Broadening — Nuisance or Lattice-Imperfections Fingerprints*

*Davor Balzar***

X-ray Laboratory, Division of Materials Science and Electronics, Department of Physics, Ruđer Bošković Institute, P.O. Box 1016, 10001 Zagreb, Croatia

Received February 15, 1996; revised June 16, 1996; accepted July 10, 1996

Diffraction lines are broadened for two reasons: instrumental configuration and physical origins. The latter yields information on materials microstructure. The complete process of line-broadening analysis is discussed, beginning with experimental procedures and a correction for instrumental broadening. In the analysis of the physically broadened line profile, the main emphasis is given to the widely used methods of separation of size and strain broadening: the Warren-Averbach approximation and integral-breadth methods. The integral-breadth methods are collated and their reliability discussed. Close attention is given to an assumed Voigt-function profile shape for both size-broadened and strain-broadened profiles because it is shown that a Voigt function fits satisfactorily the physically broadened line profiles of W and MgO obtained by the Stokes-deconvolution method. The subsequent analyses of broadening are performed by using the Warren-Averbach and »double-Voigt« approaches and results are compared.

INTRODUCTION

Depending on the particular material and specimen history, diffraction lines show some extent of broadening. In case of powder diffraction, this

* Based upon the plenary lecture presented at the 4th Croatian-Slovenian Crystallographic Meeting, Trakošćan, Croatia, September 28–30, 1995.

** On leave at the Materials Science and Engineering Laboratory, National Institute of Standards and Technology, 325 Broadway, Boulder, Colorado 80303, U.S.A.

phenomenon may cause severe line overlapping, which complicates analysis of the pattern and may lead to errors or even failure in determination and refinement of crystal structure. However, as our understanding of line-broadening origins has improved over decades, it has become clear that its analysis may yield valuable information on microstructure and defects of materials.

Phenomenological line-broadening theory of plastically deformed metals and alloys was developed by Warren.[1,2] It identifies two main types of broadening: the so-called size and strain components. The former depends on size of coherent domains (or incoherently diffracting domains in a sense that they diffract incoherently one to another), which is not limited to the grains but may include effects of stacking and twin faults and subgrain structures (small-angle boundaries, for instance), and the latter is caused by any lattice imperfection (dislocations and different point defects). The theory is general and was successfully applied to other materials, including oxides and polymers. However, the parameters obtained need a careful assessment of their physical validity and correlation to the particular structural features of material under investigation. In different approaches,[3–5] the effects of simplified dislocation configurations on diffraction-line broadening were modeled. Although these microscopic models correctly identify origins of broadening in terms of physically recognized quantities, their application is still difficult for real materials where many different sources of line broadening are usualy present simultaneously. The focus here is to study and compare methods of line-broadening analysis in the frame of phenomenological approaches.

The development of this research field goes back to 1918 when Scherrer[6] understood that small crystallites cause broadening of diffraction lines. However, more than quarter of a century was needed before a more complex and exact theory of line broadening was formulated by Stokes and Wilson.[7] They included the lattice strain as another origin of broadening. Shortly thereafter, a new impulse was given to the theory: Stokes[8] adapted the Fourier-deconvolution method to obtain the pure physically broadened line profiles from the observed pattern. Instead of mere estimations of either average size of coherent domains or some measure of strain, through the developments of Bertaut[9] and Warren and Averbach,[1,10] a more detailed analysis of complete line-profile shape was possible. Moreover, Wilson[11] introduced the analysis of the variance of profile, and Ergun[12] the method of successive foldings. All those procedures pushed aside the integral-breadth methods because of an important advantage not to be model-dependent. Moreover, with a careful application, it was possible to obtain much more information, such as column-length distribution function, the behavior of strain as a function of the averaging distance in domains, *etc*. However, they also have very serious drawbacks: In cases of large line overlapping, or weak structural broadening, the Stokes deconvolution method cannot be applied without severe errors. This limits application to a small number of speci-

mens and to cubic crystal systems. Moreover, the mathematical process involved is rather cumbersome and difficult to apply in a straightforward manner. This is why, after the development of the Rietveld refinement[13] and other full-powder-pattern-fitting techniques (Pawley,[14] Toraya[15]), the integral-breadth fitting methods became attractive again. After Langford[16] introduced a Voigt function in the field of X-ray powder diffraction, it was quickly adopted in the Rietveld analysis,[17] along with its approximations.[18] It proved to be satisfactory and flexible enough for most purposes when angle dependence of parameters is modeled properly.

On the other side, although the Stokes method has put severe limitations on the analysis, the Warren-Averbach method of separation of size-strain broadening has stayed the least constrained method for analyzing diffraction-line broadening. The parameters obtained through the Warren-Averbach and integral-breadth methods are differently defined, and thus not necessarily comparable. The main intention here is to study these two different courses of line-broadening analysis and show their equivalency under the following circumstances: both size-broadened and strain-broadened line-profiles are modeled with a Voigt function and distance-averaged strain follows the Gauss distribution.[19] The first condition also defines the total physically broadened profile as a Voigt function. The experiments were performed on W and MgO powders to study the feasibility of the simple Voigt-function modeling in line-broadening analysis. The physically broadened line profiles obtained through two different approaches, namely Stokes deconvolution and convoluted-profile fitting, are compared. Furthermore, the Warren-Averbach and integral-breadth methods are applied to the so-obtained respective physically broadened line profiles, and differences are assessed.

MEASUREMENTS AND PRELIMINARY DATA TREATMENT

Looking at the inherent sensitivity of errors in the line-broadening analysis, much attention should be paid to the preparation of specimen and collection of data as a necessary prerequisite to the subsequent analysis. Many textbooks give necessary guidelines; one of the recent ones is »Modern Powder Diffraction«.[20,21] Detailed procedures were given in an excellent review by Delhez, Keijser, and Mittemeijer.[22] The recent paper by Langford[23] gives very comprehensive guidelines for the determination of microstructural properties by pattern decomposition. Here, some hints at the most critical steps will be reviewed. The necessary requirement is a good counting statistics, much better than for full-pattern analysis like the Rietveld refinement where the whole pattern is treated simultaneously. On the other side, in the line-broadening analysis, the knowledge of relative line intensities is not required, meaning that texture and grain size are of a smaller concern. However, it is clear that the extremely poor crystal statistics does not give a complete information for the specimen on the whole, and can distort line-

profile shapes. Generally, the use of the »infinitively« thin specimen is preferred over an »infinitively« thick specimen in order to suppress a possible transparency broadening for low-absorbing compounds. However, a very thin specimen lays augments the importance of surface roughness, which introduces additional broadening.

The high-resolution experimental setup is preferable at the expense of beam intensity. Synchrotron radiation is therefore a very desirable, but most often unavailable source. For the laboratory sources, the incident-beam monochromator is not necessary, but a helpful possibility.[24] Care should be taken to minimize sources of line asymmetry (particularly the axial divergence by means of Soller slits on both sides of the specimen) because it complicates the line-broadening analysis. It is advisable to analyze the whole pattern before taking any detailed line-broadening analysis to notice possible peak shifts (indication of macrostresses and/or structural faults) and peak-width anisotropy.

DIFFRACTION-LINE BROADENING

Theoretically, intensity diffracted from an infinite crystal should consist of diffraction lines without width (Dirac delta functions) at discrete diffraction angles. However, both instrument and specimen broaden the diffraction lines, and the observed line profile is a convolution[25]

$$h(x) = g(x) \star f(x) + \text{background} \,. \tag{1}$$

Wavelength distribution and geometrical aberrations are usually treated as characteristic for the particular instrument (instrumental profile):

$$g(x) = \omega(x) \star \gamma(x) \,. \tag{2}$$

To obtain microstructural parameters of the specimen, the physically (specimen) broadened profile f must be extracted from the observed profile h.

Origins of specimen broadening are numerous. Generally, any lattice imperfection will cause additional diffraction-line broadening. Therefore, dislocations, vacancies, interstitials, substitutions, and similar defects lead to lattice strain. If a crystal is broken into smaller incoherently diffracting domains by dislocation arrays (small-angle boundaries), stacking faults, twins, large-angle boundaries (grains), or any other extended imperfections, then domain-size broadening occurs.

Instrumental broadening

The first step before any attempt to analyze the diffraction line broadening is to correct the observed line profiles for the effects of the instrument. Despite recent attempts to calculate the complete instrumental contribution

to the line broadening *ab initio*,[26,27] a careful scan of a suitable standard sample, showing a minimal physical broadening, should suffice. Thorough recipes for preparing the suitable standard specimen are given elsewhere.[28]

In the past, it was customary to anneal the specimen showing broadened reflections in order to obtain a standard. This was the most desirable approach when the Stokes deconvolution method was applied because the centroids of f and g should be as close as possible. However, very often a material does not give satisfactorily narrow lines. It is becoming more of a practice to find a suitable certified standard reference material, which allows a true comparison of results among different laboratories. Because the lines of standard and studied specimen usually do not coincide, it is required to model the characteristic parameters of standard's line-profile shapes analytically, so the needed instrumental profile can be synthesized at any angle of interest. Most often, the original Caglioti, Paoletti, and Ricci[29] relation is used:

$$\mathrm{FWHM}^2(2\theta) = U \tan^2\theta + V \tan\theta + W \ . \tag{3}$$

Although this function was derived for neutron diffraction, it was confirmed to work well also in the X-ray diffraction case. A more appropriate function for the X-ray angle-dispersive powder diffractometer, based on theoretically predicted errors of some instrumental parameters may be the following:[30]

$$\mathrm{FWHM}^2(2\theta) = W + V'\sin^2 2\theta + U \tan^2\theta + U' \cot^2\theta \ . \tag{4}$$

This function may better model the increased axial divergency at low angles and correct for the specimen transparency.[30] However, contrary to the requirement on the physically broadened line profile, most important for the instrumental function is to correctly describe the angular variation of parameters, regardless of its theoretical foundation.

It was found that U can model the wavelength dispersion,[31,32] and W the aperture of the receiving slit[32] of a synchrotron beam. By measuring the line-profile widths of a well-characterized standard flat sample, a very simple angular dependence of Cauchy and Gauss integral breadths of a fitted Voigt function was found:[32]

$$\begin{aligned} \beta_C(2\theta) &= A/\cos\theta + B \tan\theta \ ; \\ \beta_G^2(2\theta) &= C/\cos^2\theta + D \tan^2\theta \ . \end{aligned} \tag{5}$$

Here, $A \approx 0$ and $D < 0$, $|D| << B$, meaning that the Gauss part shows much smaller overall angular variation. Moreover, for the incident-beam monochromated laboratory source, Louër and Langford[24] found from Voigt-function fits to the line profiles of a standard specimen that the constituent

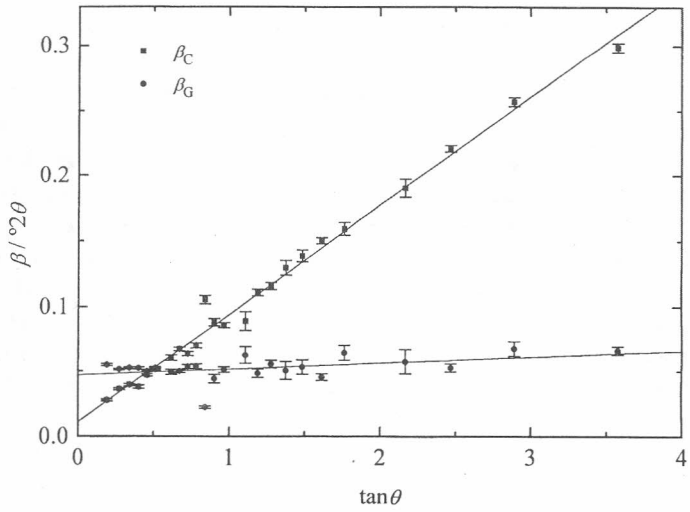

Figure 1. Cauchy and Gauss integral breadths of the Voigt function fitted to the line profiles of an »infinitely« thin specimen of NIST standard reference material 660 LaB_6.

Cauchy integral breadth increased steadily, whereas the constituent Gauss integral breadth did not change much with the diffracting angle. It was argued that the predominantly Gaussian character at low angles is due to the geometry of the diffractometer, whereas the wavelength distribution gives rise to the Cauchian character at high angles. Likewise, for the $K\alpha_1 + K\alpha_2$ laboratory source, a similar behavior was found[33] (see Figure 1). Therefore, in the first approximation, the instrumental broadening could be estimated from a measurement at only one angle:

$$\beta_C(2\theta) = a \tan\theta \; ; \quad \beta_G(2\theta) = b \; . \tag{6}$$

Extraction of physically broadened line profile

A choice of the method to obtain the parameters of pure physically broadened line profiles is of utmost importance for the subsequent line-broadening analysis. Basically, the methods used can be divided in two groups: (i) Deconvolution approach where the physically broadened line profile is unfolded from the observed profile using the previously determined instrumental profile; (ii) Convolution approach, that is, contrary to the former, the observed profile is built according to (1) and adjusted to the observed pattern through a least-squares fitting. However, we have a knowledge of h and g, but not of f. Therefore, both the general type and

parameters of f are assumed, which introduces a bias in the method. On the other side, with development of the Rietveld and similar algorithms, where all the parameters are determined in this way anyhow, this approach can be built into the code in parallel to the structural and other parameters and refined simultaneously, whereas deconvolution procedures are much more complicated to introduce. Another important difference between the two approaches is that deconvolution methods at some circumstances either fail or become unstable and inaccurate.[34] The convolution process is always stable, but, besides the systematic errors introduced by a possible inadequate model of physically broadened line profile, the iterative least-squares minimization procedure can be trapped in the false minimum. Moreover, the smallest reliability index does not necessarily correspond to a physically meaningful solution; for instance, adding more peaks in refinement than actually exist may decrease it. For some illustrations and possible artifacts of profile fitting see Howard and Preston,[35] and for an example of how a high degree of line overlap may influence size-strain analysis see Balzar.[36]

The most used of the first type is the Fourier-transform deconvolution method,[8] although there are some novel approaches[37] using constrained Phillips-Twomey[38] or maximum-entropy[39] deconvolution methods. Another, in fact deconvolution process, although accomplished by easy substraction of the instrumental-profile variance[11] is not used extensively, and will not be considered here. Likewise, among the methods falling in the second group, the iterative method of successive foldings[12] is used sparingly, and it will not be considered. Some new developments can be found in the review by Reynolds.[40] The most widely used in the convolution-fitting approach are the integral-breadth methods. They will be treated extensively here.

Deconvolution method of Stokes

From (1), it follows that deconvolution can be performed easily in terms of complex Fourier transforms of respective functions:

$$F(n) = \frac{H(n)}{G(n)} . \tag{7}$$

The inverse Fourier transform gives back a physically broadened line profile:

$$f(x) = \sum_n \frac{H(n)}{G(n)} \exp\left(-\frac{2\pi i x n}{x_m}\right) . \tag{8}$$

Hence, the physically broadened profile f is retrieved from the observed profile h without any assumption (bias) on the peak-profile shape. However, (7) may not give a solution if the Fourier coefficients of the f profile do not van-

ish before those of the g profile.[41] Furthermore, if physical broadening is small compared with instrumental broadening, deconvolution becomes too unstable and inaccurate. If the h profile is 20 % broader than the g profile, this gives an upper limit of about 1000 Å for the determination of the effective domain size.[42] Regardless of the degree of broadening, deconvolution produces unavoidable profile-tail ripples because of truncation effects. To obtain reliable results, errors of incorrect background, sampling, and the standard specimen have to be corrected.[41,43,44] The largest conceptual problem, however, is peak overlapping. If the complete peak is not separated, the only possible solution is to try to reconstruct the missing parts. This would require some assumption on the peak-profile shape, that is introduction of bias into the method. The application of the strict Stokes method is therefore limited to materials having the highest crystallographic symmetry.

Convolution-fitting methods

Here it is required that at least the unknown physically broadened diffraction profile f be approximated with some analytical function. In the past, two commonly used functions were Gauss

$$I(x) = I(0) \exp\left(-\pi \frac{x^2}{\beta_G^2}\right) \tag{9}$$

and Cauchy (Lorentz)

$$I(x) = I(0) \frac{1}{\frac{\beta_C^2}{\pi^2} + x^2} . \tag{10}$$

From the convolution integral (1), it follows that for Cauchy profiles

$$\beta_{hC} = \beta_{gC} + \beta_{fC} \tag{11}$$

and for Gauss profiles

$$\beta_{hG}^2 = \beta_{gG}^2 + \beta_{fG}^2 . \tag{12}$$

However, the observed X-ray diffraction line profiles can not be well represented with a simple Cauchy or Gauss function.[18,45] But they are almost pure Cauchy at highest angles because the dominant cause of broadening becomes the spectral distribution in radiation. Different geometrical aberrations of the instrument are difficult to describe with simple analytical functions. In the case of closely Gaussian broadening of γ, following (2), the

instrumental line profile can be best described by a convolution of Cauchy and Gauss functions, which is the Voigt function. Experience shows that the Voigt function (or its approximations, pseudo-Voigt[46] and Pearson-VII[47]) also fits very well the observed peak profiles. The Voigt function is usually represented following Langford:[16]

$$I(x) = I(0)\left(\frac{\beta}{\beta_C}\right) \mathrm{Re}\left[\mathrm{erfi}\left(\frac{\pi^{1/2}x}{\beta_G} + ik\right)\right]. \tag{13}$$

Here, the complex error function is defined as

$$\mathrm{erfi}(z) = \exp(-z^2)\,\mathrm{erfc}(-iz) \tag{14}$$

and erfc denotes the complementary error function.

Integral breadth of the Voigt function is expressed through its constituent integral breadths[48]

$$\beta = \beta_G \frac{\exp(-k^2)}{\mathrm{erfc}(k)} \tag{15}$$

Halder and Wagner[49] showed that the following parabolic expression is a satisfactory approximation:

$$\beta^2 = \beta_C\beta + \beta_G^2 . \tag{16}$$

Because convolution of two Voigt functions is also a Voigt function, integral breadths are easily separable conforming to (11) and (12).

In case that any of h, g, or f profiles are asymmetric, they cannot be modeled with the discussed functions. Indeed, for Bragg-Brentano geometry, observed diffraction-line profiles are asymmetric toward the low-angle side for small diffraction angles and switch to a slight reverse asymmetry at the highest diffraction angles. Asymmetry is introduced in g by axial beam divergency, specimen transparency and flat surface.[45] However, the extrinsic stacking and twin faults may introduce (relatively weak) asymmetry in f also.[50] Unfortunately, numerical convolutions are usually necessary in these cases, thus consuming calculation time and introducing additional errors. This is why asymmetry is often neglected. However, it may cause large errors in line-broadening analysis. Some examples of numerical convolutions used are the following: Enzo *et al.*[51] modeled g with a pseudo-Voigt convoluted with the exponential function and f with a pseudo-Voigt; Howard and Snyder[52] modeled g with a split-Pearson VII and f with a Cauchy function, whereas Balzar[36] modeled g also with a split-Pearson VII but f with a Voigt function. There were no attempts yet to assume the asymmetrical f profile.

Physically broadened profiles of W and MgO

It was mentioned that the Stokes Fourier-deconvolution method followed by the Warren-Averbach analysis of physically broadened line profile is the least biased approach to the analysis of line broadening. The opposite procedure is profile fitting of the convolution of the presumed analytical function, modeling the physically broadened line profile, and instrumental profile obtained by measuring a suitable standard material and consecutive application of some integral-breadth method. Both approaches have both drawbacks and advantages and it is generally assumed that different results are obtained. The critical step is a correction for instrumental broadening. Because of numerous problems associated with the Fourier deconvolution and especially the inevitable ripples at tails of physically broadened profile, there were almost no attempts to fit it with some analytical function. Suortti, Ahtee, and Unonius[53] fitted a Voigt function to the least-squares deconvoluted profiles of a Ni powder and found a good overall agreement. Reynolds[40] fitted successfully a pseudo-Voigt function to the physically broadened line profiles of chlorite, obtained by the Ergun method of iterative folding.[12] Although different approaches to deconvolution are possible, we used the Stokes method because of its wide acceptance. Many different integral-breadth routes were used in the literature. We followed our previous studies.[36]

Materials

Two »classical« materials for line-broadening analysis, W and MgO, were selected because of their simple cubic structure (the Stokes method is optimally applicable) and different origins of broadening: It is expected that on cold deformation W shows dominantly strain broadening caused by introduction of numerous dislocations, whereas the thermal decomposition of $MgCO_3$ gives rise to size broadening only. W is elastically isotropic and shows well-resolved reflections thus admitting a relatively large number of reflections to be analyzed simultaneously. Likewise, because of negligible strain and low probability of fault formation in MgO, a simultaneous treatment of all accessible reflections is possible. W powder of nominal size 8–12 μm was submitted to ball-milling for different times, although after some initial milling time no additional change of peak widths was observed. The fine $MgCO_3$ powder was decomposed at different temperatures, 350 °C and higher. The powder was kept at a particular temperature for 3 hours and allowed to cool slowly in the furnace to minimize possible lattice defects. As a standard specimen for W, the original untreated W powder was used. It shows minimal line broadening, comparable to the NIST standard reference material LaB_6. As a standard for MgO, the MgO powder decomposed at 1300 °C for 6 hours was used. Although it showed relatively broad reflections

(FWHM at 37° 2θ was about 0.15° 2θ compared to only 0.08° 2θ for LaB_6), we used it to get optimal conditions for the Stokes analysis, because the appreciable difference between standard and specimen peak positions represents a problem, and the needed interpolation of Fourier coefficients of the standard would introduce additional uncertainties. Moreover, we were not interested in the absolute magnitude of results. We chose specimens from each batch (W specimen ball milled for 140 min and MgO specimen decomposed at 550 °C) showing approximately 3–4 times broader reflections than the respective standards, because the Stokes method has optimum application for this factor in the range 2–6.[34]

Data analysis

Data were collected using a horizontal goniometer and counted with a solid-state detector. We used a fixed-time counting method with a condition to collect about 10000 counts at each peak maximum. The raw data were used in analysis to avoid introducing any bias by smoothing methods. However, the deconvolution process is very sensitive to the noise in the data and it caused unwanted spurious oscillations in Fourier coefficients. We measured seven W reflections using Cu $K\alpha$ radiation. The 400 peak was excluded because the high-angle background was not accessible with our goniometer. For the MgO pattern, we analyzed only 220, 400, and 422 reflections, because others come in close pairs for the *fcc* structure. The inevitable line overlapping would require the unsafe estimation of missing tails and introduce unwanted bias in the Fourier deconvolution. Linear background was determined by fitting the first-order polynomial to data before applying either Stokes deconvolution or profile fitting. The $K\alpha_2$ elimination prior to the Stokes deconvolution was not performed because it may introduce additional errors. In the convolution-fitting approach, the $K\alpha_2$ component is treated analogously to $K\alpha_1$, but with half its intensity and the same profile shape. After correction for the Lorentz-polarization factor, Stokes deconvolution was performed on a 2θ scale to be in accord with the profile fitting. Hence, for both deconvolution and fitting/convolution approaches, there is a systematic error because the subsequent analyses are implemented in Fourier space. Although it is possible to perform both Stokes deconvolution and profile fitting on the s scale, we found the error to be negligible at this or a smaller level of broadening. The origin was taken at the centroid of the standard peak, although there were no substantial shifts of broadened peaks. The convolution-fitting process was performed in the following way: Instrumental profile was obtained by fitting the split-Pearson VII function to the particular line profile of standard specimen. By convoluting it with the preset physically broadened Voigt function, the »observed« profile is obtained. After adding the prerefined linear background, the parameters of

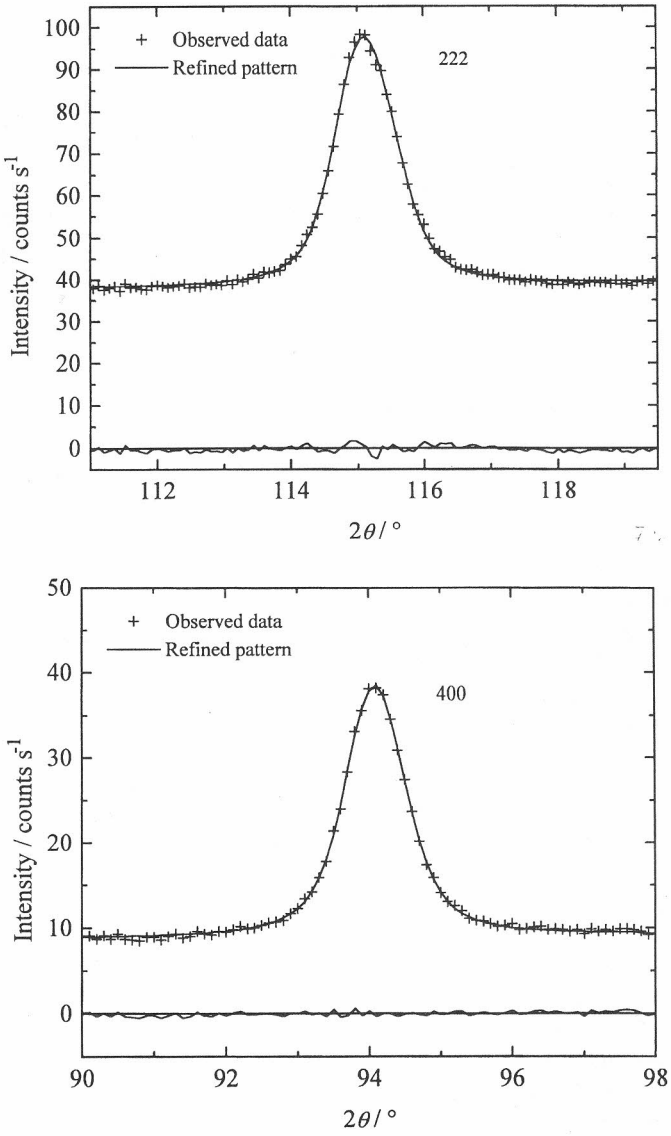

Figure 2. Fits to the observed line profile of the convolution of instrumental split-Pearson VII function and the Voigt physically broadened profile for the least intense peaks of W and MgO. Difference patterns plotted around zero intensity on the same scale: (a) 222 W; (b) 400 MgO.

physically broadened Voigt function are adjusted in the least-squares fitting to the observed pattern. Typical plots are given in Figure 2.

Fitting of physically broadened line profiles

Following (8), the physically broadened line profile can be back-synthesized from the Fourier coefficients obtained by deconvolution. However, because of noise in raw data, after some harmonic number, Fourier coefficients become unreliable causing large oscillations in the synthesized profiles.[41] We monitored the change of all Fourier coefficients with the harmonic number and found that the most reliable indicator is behavior of real Fourier coefficients. After the initial decrease, they very often oscillate around zero, followed by an increase. Therefore, we cut off the synthesis at a particular harmonic number when real Fourier coefficients reach zero. Typical plots of

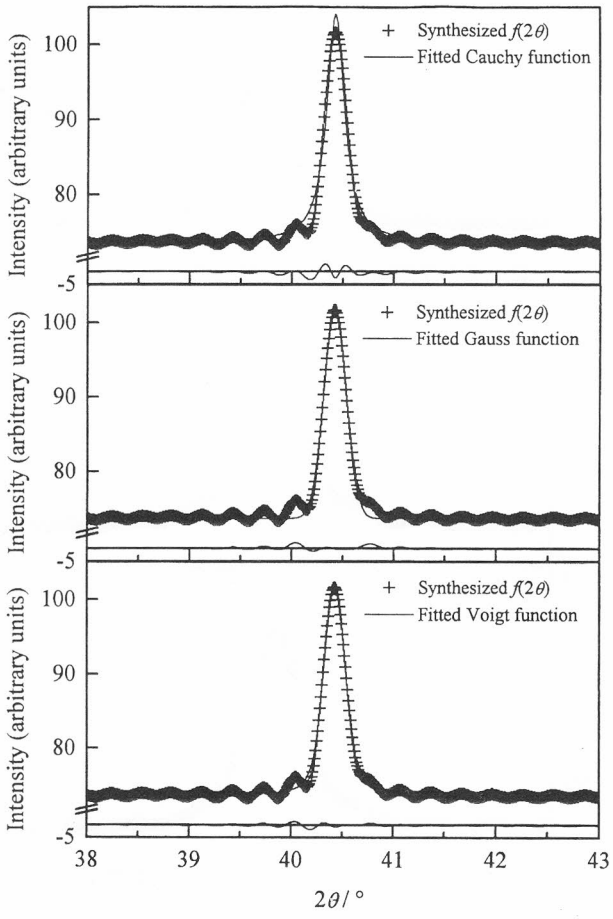

Figure 3. Cauchy, Gauss, and Voigt-function fits to the Stokes-deconvoluted physically broadened 110 W line profile. Difference patterns plotted around zero intensity on the smaller scale.

synthesized physically broadened line profiles are shown in Figures 3 and 4 along with their least-squares fits of Cauchy, Gauss, and Voigt functions. The complete results for both materials are presented in Tables I and II. It is evident that the lowest residual indexes are obtained for a Voigt-function fit despite fewer free parameters. Even more important is how different functions fit profiles. While the Cauchy function approximates tails quite well, it fails to resemble profile shape close to its maximum. On the contrary, the Gauss function fits fairly well around the peak maximum, whereas tails fall off too rapidly. This is known to be true also for the observed diffraction profiles.

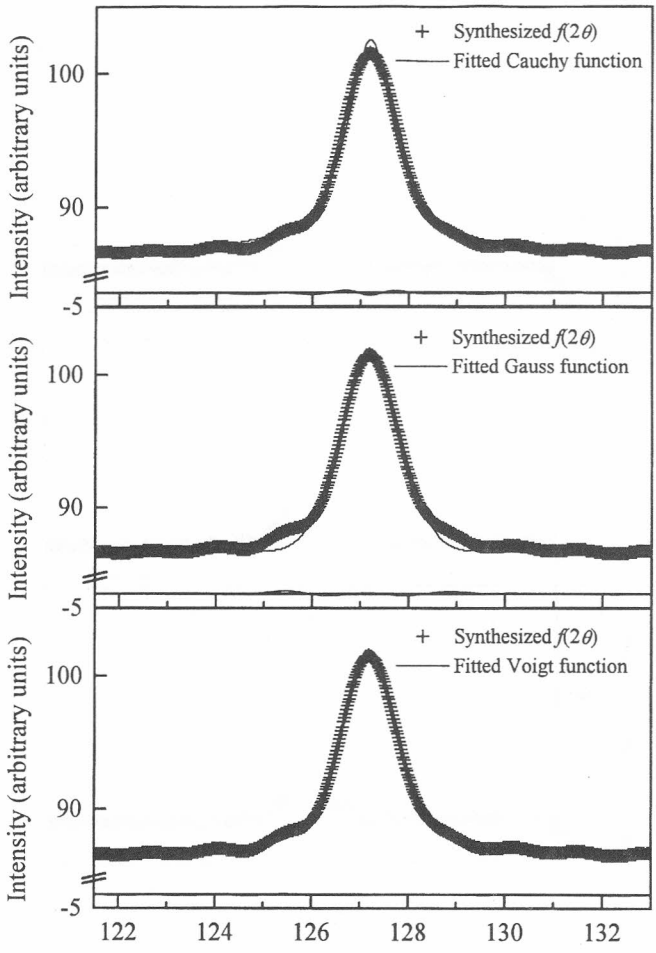

Figure 4. Cauchy, Gauss, and Voigt-function fits to the Stokes-deconvoluted physically broadened 422 MgO line profile. Difference patterns plotted around zero intensity on the smaller scale.

TABLE I

Least-squares fits to the synthesized physically broadened line profiles of W obtained by the Fourier-deconvolution Stokes method[8]

hkl	Voigt function					Cauchy function		Gauss function	
	β_C ° 2θ	β_G ° 2θ	β ° 2θ	FWHM ° 2θ	R_{wp} %	FWHM ° 2θ	R_{wp} %	FWHM ° 2θ	R_{wp} %
110	0.141(5)	0.207(3)	0.306	0.250	0.37	0.208(2)	0.64	0.260(1)	0.49
200	0.237(5)	0.221(3)	0.394	0.302	0.29	0.259(2)	0.47	0.328(2)	0.49
211	0.416(6)	0.222(5)	0.544	0.384	0.30	0.347(2)	0.35	0.452(2)	0.52
220	0.460(8)	0.301(6)	0.649	0.472	0.30	0.415(2)	0.37	0.544(3)	0.49
310	0.664(17)	0.190(21)	0.732	0.485	0.55	0.469(5)	0.55	0.620(6)	0.73
222	0.647(17)	0.610(12)	1.083	0.831	0.32	0.690(4)	0.39	0.925(4)	0.41
321	1.243(15)	0.460(15)	1.452	0.984	0.21	0.921(4)	0.23	1.224(7)	0.42

TABLE II

Least-squares fits to the synthesized physically broadened line profiles of MgO obtained by the Fourier-deconvolution Stokes method[8]

hkl	Voigt function					Cauchy function		Gauss function	
	β_C ° 2θ	β_G ° 2θ	β ° 2θ	FWHM ° 2θ	R_{wp} %	FWHM ° 2θ	R_{wp} %	FWHM ° 2θ	R_{wp} %
220	0.427(9)	0.576(6)	0.877	0.708	0.18	0.595(4)	0.39	0.742(3)	0.30
400	0.805(22)	0.593(16)	1.196	0.885	0.33	0.780(6)	0.40	0.984(7)	0.47
422	1.056(13)	1.024(9)	1.794	1.383	0.15	1.184(6)	0.32	1.502(6)	0.32

In Tables III and IV we compare the parameters of so-obtained Voigt-function fits to the Voigt function used to model physically broadened line profiles through the convolution fitting. Except for two low-angle W lines, both Cauchy and Gauss, and particularly the total integral breadths, agree very well. This discrepancy at low angles is not understood at present, because the instrumental-profile asymmetry was modeled in convolution-fitting approach.

One may conclude that it seems reasonable to approximate the physically broadened line profile with a Voigt function. Because a convolution of two Voigt function is also a Voigt function, in the subsequent paragraphs we shall emphasize use of a Voigt function both as a size-broadened and a strain-broadened profile in line-broadening analysis.

TABLE III

Comparison of Voigt-function fits to the synthesized physically broadened line profiles of W obtained by the Fourier-Stokes deconvolution method (S.D.) (Table I) and an assumed physically broadened Voigt profile used in convolution-fitting (C.F.) approach. The agreement index is defined as $R = 100 - 100\ \beta(\text{C.F.})/\beta(\text{S.D.})$.

hkl	β_C (S.D.) ° 2θ	β_C (C.F.) ° 2θ	β_G (S.D.) ° 2θ	β_G (C.F.) ° 2θ	β (S.D.) ° 2θ	β (C.F.) ° 2θ	R %
110	0.141(5)	0.222(4)	0.207(3)	0.114(7)	0.306	0.286	6.5
200	0.237(5)	0.276(4)	0.221(3)	0.166(6)	0.394	0.377	4.3
211	0.416(6)	0.408(6)	0.222(5)	0.220(9)	0.544	0.535	1.7
220	0.460(8)	0.443(11)	0.301(6)	0.319(13)	0.649	0.651	–0.3
310	0.664(17)	0.567(11)	0.190(21)	0.318(16)	0.732	0.754	–3.0
222	0.647(17)	0.629(33)	0.610(12)	0.633(31)	1.083	1.089	–0.6
321	1.243(15)	0.982(25)	0.460(15)	0.746(29)	1.452	1.479	–1.9

TABLE IV

Comparison of Voigt-function fits to the synthesized physically broadened line profiles of MgO obtained by the Fourier-Stokes deconvolution method (S.D.) (Table II) and an assumed physically broadened Voigt profile used in convolution-fitting (C.F.) approach. The agreement index is defined as $R = 100 - 100\ \beta(\text{C.F.})/\beta(\text{S.D.})$.

hkl	β_C (S.D.) ° 2θ	β_C (C.F.) ° 2θ	β_G (S.D.) ° 2θ	β_G (C.F.) ° 2θ	β (S.D.) ° 2θ	β (C.F.) ° 2θ	R %
220	0.427(9)	0.638(13)	0.576(6)	0.381(17)	0.877	0.869	0.9
400	0.805(22)	0.803(28)	0.593(16)	0.563(28)	1.196	1.167	2.4
422	1.056(13)	1.140(42)	1.024(9)	0.999(42)	1.794	1.838	–2.5

SIZE-STRAIN ANALYSIS

After removing the instrumental broadening from the observed line profile, it is possible to analyze the physically broadened line profile, to consider the origins and amount of broadening. A classical review about Fourier methods and integral-breadth methods was given by Klug and Alexander.[45] A survey of single-line methods was authored by Delhez, de Keijser, and Mittemeijer.[22] The use of variance (reduced second moment of the line profile) in the analysis of broadening is nowadays sparingly used and will not be treated here. Opposed to these methods, some alternative approaches may prove to be advantageous. Even though the Fourier deconvolution or similar method is rather awkward to introduce in any full-powder-pattern-fitting program, the so-called Rietveld-Fourier approach introduced by Le Bail[54] solves this problem by describing line profiles with the coefficients in Fourier space. Hence, any contribution to the line broadening is accomplished by simple multiplication of coefficients. Furthermore, an information (entropy) approach[55] was used to obtain column-length distribution functions, and recently it was demonstrated that a Monte Carlo interference-function-fitting approach[56] gives an alternate route to the Stokes deconvolution and Warren-Averbach analysis.

It was discussed[44] that »size« and »strain« terms can be applied only tentatively. The size broadening describes all the possible effects that could be put under the common denominator »coherent domain size«, that is, the size of domains distinctly defined by incoherent diffraction, such as stacking (deformation) or twin (growth) faults, small-angle boundaries caused by dislocation ordering, grains, or similar extended lattice defects. This is why X-ray domain size sparingly amounts to the particle or grain size, measurable by other, mostly optical, methods (microscope, laser-size analyzer, *etc.*). On the other side, the strain term includes contributions from any disruption of a regular lattice, such as dislocations and different point defects. It follows that these two effects are interconnected; dislocations cause strain but also arrange into boundaries between incoherently diffracting domains. This is one of the reasons why any interpretation of the underlaying physics of broadening is difficult.

Most of the work on X-ray diffraction line broadening was done on metals and alloys. Nowadays, it is widely accepted that plastic deformation in metals produces dislocation arrays, which divide crystallites into much smaller incoherently scattering domains. These dislocations produce a strain within the domains, causing strain broadening. In nonmetallic samples, the origins of broadening are somewhat different. Very often it is disregarded that, in the frame of current line-broadening theories, lattice strain is affected by other lattice imperfections, such as substitutions, vacancies, interstitials, site disorder, *etc.* Although these effects in nonmetallic materials are often of a smaller importance than the size effect, only after a careful analy-

sis it is possible to judge when some effects become »negligible«. Therefore, it will be assumed throughout this chapter that both size and strain broadening are present simultaneously. Then, the physically broadened line profile is a convolution of size-broadened and strain-broadened line profiles.

Size broadening

Scherrer[6] gave a basic definition of the »apparent« domain size

$$\langle D\rangle_v = \frac{K\lambda}{\beta_S(2\theta)\cos\theta}; \quad \langle D\rangle_v = \frac{1}{\beta_S}. \tag{17}$$

The constant K depends on the crystallite shape,[57] but generally is close to unity. It is clear that size broadening is independent of the reflection order, that is, independent of diffraction angle. This measure of domain size is a volume-weighted quantity.

Bertaut[9,58] and Warren and Averbach[1] independently derived another definition of domain size, the surface-weighted average. The Warren-Averbach method was developed originally for plastically deformed metals, but since its introduction it found a successful application to many other materials. The method is extensively described in Warren's publications.[2,50] Each domain is represented by columns of cells along the $\boldsymbol{a}_3$ direction normal to the diffracting planes ($00l$). All variables here are expressed as functions of column length $L = n|\boldsymbol{a}_3|$, which is assumed to be positive, being a distance in real space between a pair of cells along direction of $\boldsymbol{a}_3$. The size coefficient then reads[59]

$$A_S(L) = \int_L^\infty \left(1 - \frac{L}{L'}\right) p_v(L')\,\mathrm{d}L' = \frac{1}{\langle D\rangle_s}\int_L^\infty (L' - L)\, p_s(L')\,\mathrm{d}L', \tag{18}$$

because it holds that

$$p_v(L) = \frac{L}{\langle D\rangle_s} p_s(L). \tag{19}$$

Here, the average surface-weighted domain size and the surface-weighted and volume-weighted column-length distribution functions are

$$\left(\frac{\mathrm{d}\,A_S(L)}{\mathrm{d}\,L}\right)_{L\to 0} = -\frac{1}{\langle D\rangle_s}; \tag{20}$$

$$p_s(L) \propto \frac{\mathrm{d}^2 A_S(L)}{\mathrm{d}\,L^2}; \quad p_v(L) \propto L\frac{\mathrm{d}^2 A_S(L)}{\mathrm{d}\,L^2}. \tag{21}$$

For a Voigt size-broadened profile, the size coefficient is given as a Fourier transform of (13):

$$A_S(L) = \exp(-2L\beta_{CS} - \pi L^2\beta_{GS}^2) . \tag{22}$$

By differentiating it twice, we obtain

$$\frac{d^2 A_S(L)}{d L^2} = \left[(2\pi L\beta_{GS}^2 + 2\beta_{CS})^2 - 2\pi\beta_{GS}^2\right] A_S(L) . \tag{23}$$

Selivanov and Smislov[60] showed that this may be a satisfactory approximation for some size-distribution functions.

If the column-length distribution functions are known, it is possible to evaluate mean values of respective distributions:

$$\langle D\rangle_{s,v} = \frac{\int_0^\infty L p_{s,v}(L)\, d L}{\int_0^\infty p_{s,v}(L)\, d L} . \tag{24}$$

Integrals of this type can be evaluated analytically:[61]

$$\int_0^\infty z^m \exp(-bz^2 - cz)\, d z = \frac{(-1)^m}{2}\left(\frac{\pi}{b}\right)^{\frac{1}{2}} \frac{\partial^m}{\partial c^m}\left[\exp\left(\frac{c^2}{4b}\right)\operatorname{erfc}\left(\frac{c}{2\sqrt{b}}\right)\right], \tag{25}$$

and for surface-weighted and volume-weighted domain size it follows that

$$\langle D\rangle_s = \frac{1}{2\beta_{CS}} ; \quad \langle D\rangle_v = \frac{\exp(k_S^2)}{\beta_{GS}} \operatorname{erfc}(k_S) = \frac{1}{\beta_S} . \tag{26}$$

The same value of $\langle D\rangle_s$ is found from (20) and $\langle D\rangle_v$ is consistent with the Scherrer equation (17).

Two interesting points emerge here. From (23), it is clear that the second derivative of size coefficients, and consequently column-length distribution functions, can take negative values. Because any distribution function is, by definition, always positive, the Cauchy part in the size-broadened integral breadth must dominate. Inspection of (23) shows that for small L one must require

$$\beta_{CS} \geq (\pi/2)^{1/2}\beta_{GS} . \tag{27}$$

Otherwise, the »hook« effect will occur in a plot of size coefficients $A_S(L)$ versus L, that is, the plot will be concave downward for small L (Figure 5). The »hook« effect is a widely encountered problem in the Fourier analysis of line broadening, which results in overestimation of effective domain size. It is usually attributed to experimental errors connected with the truncation of the line profiles, and consequently the overestimation of background.[62] That is consistent with (27): If too high a background is estimated, it will cause the underestimation of the Cauchy content of the Voigt fitting function because the long tails will be truncated prematurely. This proves that the preset specimen-broadening function does not necessarily eliminate the »hook« effect. An important consequence of the »hook« effect is that domain sizes calculated from distribution functions (24) will not agree with values obtained from the integral breadths (26). Figure 5 shows that $\langle D \rangle_s$ is obtained

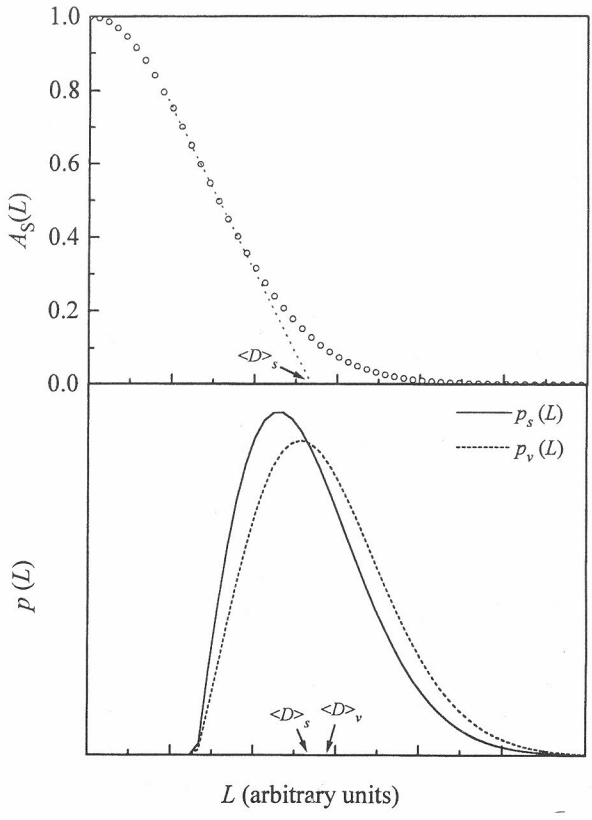

Figure 5. The »hook« effect in the plot of size coefficients occurs because the Cauchy part of the fitting Voigt function is underestimated. This causes negative values (set to zero) of the column-length distribution functions for small L.

either as the intercept on the L axis of the straight portion of $A_S(L)$ or by the numerical integration of only the positive values of the surface-weighted column-length distribution function. However, so-obtained $\langle D \rangle_s$ is erroneous as well as the value from (26), and the correct background should be found.

Another thing requiring a closer attention is the ratio of volume-weighted to surface-weighted domain size. Using (19) and (24) it follows that

$$\langle D \rangle_v = \frac{\langle D^2 \rangle_s}{\langle D \rangle_s} . \tag{28}$$

The Schwarz inequality requires that $\langle D^2 \rangle_s \geq \langle D \rangle_s^2$, which determines that

$$\langle D \rangle_v \geq \langle D \rangle_s . \tag{29}$$

It is interesting to see the minimum value of this ratio for a Voigt size-broadened profile. From (26), using the physical solution of parabolic equation (16) for breadth of the Voigt function, it follows that

$$\frac{\langle D \rangle_v}{\langle D \rangle_s} = 2 \frac{\beta_{CS}}{\beta_S} = 4 \frac{\beta_{CS}}{\beta_{CS} + (\beta_{CS}^2 + 4 \beta_{GS}^2)^{1/2}} . \tag{30}$$

Strictly, the size-broadened profile can shift between Cauchy and Gauss extremes. After taking the inequality (27) into consideration, the ratio is bounded to the region

$$1.39 \leq \frac{\langle D \rangle_v}{\langle D \rangle_s} \leq 2 . \tag{31}$$

The more accurate lower limit is obtained from (26):

$$\frac{\langle D \rangle_v}{\langle D \rangle_s} = 2 \sqrt{\pi} k_S \exp(k_S^2) \operatorname{erfc}(k_S) . \tag{32}$$

Generally, k can also change from zero to infinity. However, the minimum allowed value of k is determined by (27):

$$\frac{1}{\sqrt{2}} \leq k_S < \infty . \tag{33}$$

This implies that the ratio of domain sizes can change in a range

$$1.31 \approx (2\pi e)^{1/2} \operatorname{erfc}\left(\frac{1}{\sqrt{2}}\right) \leq \frac{\langle D \rangle_v}{\langle D \rangle_s} < 2 . \tag{34}$$

Therefore, for a Voigt size-broadened profile, the ratio of volume-weighted to surface-weighted domain size cannot be larger than 2. At this limit, $\langle D\rangle_v = 2\langle D\rangle_s$, and the size broadening is given only by the Cauchy component. This is a case of pure Cauchy size broadening described earlier.[49,63] On the other side, if the ratio is smaller than ~1.31, the Cauchy content of the Voigt size-broadened profile was underestimated. This is an indication of incorrect background and the »hook« effect. It may be noted that most experiments give the ratio $\langle D\rangle_v / \langle D\rangle_s$ in the specified range (see for instance the review by Klug and Alexander[45]).

Strain broadening

Stokes and Wilson[7] defined an »apparent« strain as

$$\eta = \beta_D(2\theta)\cot\theta \,. \tag{35}$$

The so-called maximum (upper-limit) strain is derived as

$$e = \frac{\Delta d}{d} = \frac{\eta}{4} = \frac{\beta_D(2\theta)}{4\tan\theta}\,; \quad e = \frac{\beta_D}{2s}\,. \tag{36}$$

It was objected[64] that the strain e has a doubtful meaning because it takes only the maximum value, that is, there is no strain distribution that would be expected in a real material. Stokes and Wilson[7] defined also a root-mean-square (RMS) value of strain e_{RMS} on the assumption of a Gauss strain distribution, which differs from e by a constant factor only: $e_{RMS} = (2/\pi)^{1/2} e$. From (36) it is clear that strain broadening is angle dependent, hence it will depend on the reflection order.

The RMS strain was not used extensively in the integral-breadth methods, but was adopted later in the Fourier Warren-Averbach approach.[1] Note that these two RMS values of strain are equal only in the case of a Gaussian strain distribution, as will be explained later. If L is the undistorted distance, and distortion changes distance by ΔL, the component of strain in the $\boldsymbol{a}_3$ direction (orthogonal to reflecting planes) averaged over cell-separation distance L can be defined as $\epsilon(L) = \Delta(L)/L$. It defines the distortion coefficients of the physically broadened line profile:

$$A_D(L,s) = \langle \exp(2\pi i s L \epsilon(L))\rangle \,. \tag{37}$$

To obtain the strain component, it is necessary to approximate the exponential term. For not too large L the following approximation is useful:

$$\langle \exp(2\pi i s L \epsilon(L))\rangle \approx \exp(-2\pi^2 s^2 L^2 \langle \epsilon^2(L)\rangle) \,. \tag{38}$$

This relationship is exact if the strains $\epsilon(L)$ are distributed around the mean value according to the Gauss error function for all L values. In general

it is valid up to the terms in $\epsilon^3(L)$ because it is expected that the strain distribution is symmetrical.[7]

Analogous to the size coefficient (22), strain (distortion) coefficient of a Voigt strain-broadened profile (13) is

$$A_D(L) = \exp(-2L\beta_{CD} - \pi L^2\beta_{GD}^2) . \tag{39}$$

Then, comparison with (38) gives

$$<\epsilon^2(L)> = \frac{1}{s^2}\left(\frac{\beta_{GD}^2}{2\pi} + \frac{\beta_{CD}}{\pi^2}\frac{1}{L}\right). \tag{40}$$

Therefore, the mean-square strain decreases linearly with the averaging distance L. The expression for strain has both the L-dependent and L-independent contributions:

$$<\epsilon_V^2(L)> = <\epsilon_G^2> + <\epsilon_C^2(L)> \tag{41}$$

where

$$<\epsilon_G^2> = \beta_{GD}^2/(2\pi s^2) ; \quad <\epsilon_C^2(L)> = S_C/L ; \quad S_C = \beta_{CD}/(\pi s)^2 . \tag{42}$$

Wang, Lee, and Lee[65] used (39) to model dislocation line broadening. Adler and Houska[66] and Houska and Smith[67] demonstrated that MSS can be represented by the sum of two terms, given by Cauchy and Gauss strain-broadened profiles. Gaussian constant-strain term may describe the uniform strain throughout domains caused by either fluctuation in the density of embedded atoms[66] or by dislocation-cell walls.[68] The Cauchy part is determined by strains around individual dislocations.[69] The Cauchy parameter S_C defines the skewness of the $<\epsilon_V^2(L)>$ curve for small L. Physically, it represents the »Cauchy-strain strength«. For larger distances L, mean-square strain saturates at the pure-Gauss value $<\epsilon_G^2>$. In the case of the pure-Gauss strain broadening ($\beta_{DC} = 0$), the MSS is independent of L (see also[49,63]):

$$<\epsilon^2>^{1/2} = \left(\frac{2}{\pi}\right)^{1/2} e . \tag{43}$$

There is no obvious connection between RMSS and e if the strain-broadened line profile contains the Cauchy component. However, in the case of the pure-Cauchy strain-broadened line profile, with (36), which is assumed regardless of the particular line-profile function, and (40), it follows that the two measures of strain are related:

$$e = (\pi^2/2)Ls<\epsilon_C^2(L)> . \tag{44}$$

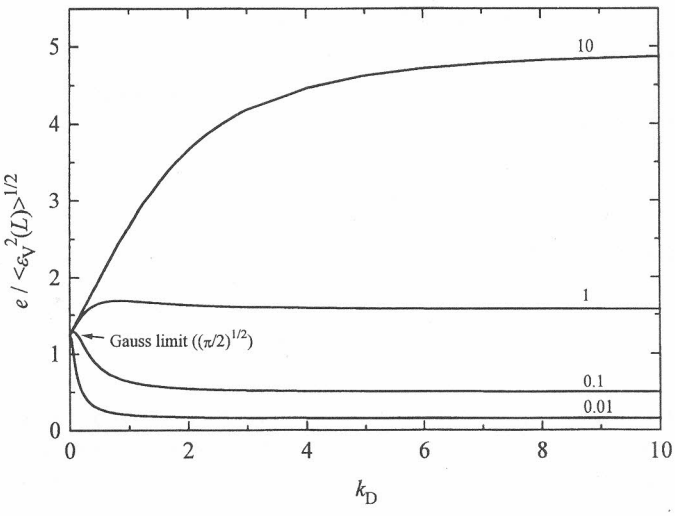

Figure 6. Ratio of maximum strain, e, to the RMSS, $\langle\epsilon^2_V(L)\rangle^{1/2}$, as a function of the Voigt parameter, $k_D = \beta_{CD}/(\pi^{1/2}\beta_{GD})$, for different values of the product $\beta_{CD}L$.

In the general case, the maximum strain e is determined from the integral breadth of a Voigt function:

$$2es = \beta_{GD}\exp(-k_D^2)/\operatorname{erfc}(k_D)\,. \tag{45}$$

In combination with (40) it follows that

$$\frac{e}{\langle\epsilon^2_V(L)\rangle^{1/2}} = \left(\frac{\pi}{2}\right)^{1/2}\frac{\exp(-k_D^2)}{\operatorname{erfc}(k_D)}\frac{1}{\left(1+\dfrac{2k_D^2}{\beta_{CD}L}\right)^{1/2}}\,. \tag{46}$$

This function is plotted in Figure 6 for different values of the product $\beta_{CD}L$. In the Gauss limit ($k_D \to 0$), the ratio is constant, $(\pi/2)^{1/2}$, as pointed above. It is interesting to consider the ratio when the Cauchy part dominates. Clearly, the ratio of strains can be either larger or smaller than unity, which depends on values of both β_{CD} and L. Let us make the reasonable estimate for the most common values for the Cauchy extreme. For large k_D, the asymptotic expansion of the complementary error function may be used:[70]

$$\pi^{1/2}z\,\exp(z^2)\operatorname{erfc}(z) \sim 1 + \sum_{m=1}^{\infty}(-)^m(1\cdot 3\cdot 5\cdot\cdots(2m-1))/(2z^2)^m\,. \tag{47}$$

We write (47) with k_D as

$$\operatorname{erfc}(k_D) = (\exp(-k_D^2)/\pi) \sum_{m'=0}^{m-1} (-)^{m'} \Gamma(m' + 1/2)/k_D^{(2m'+1)} + R_m(k_D^{-(2m+1)}) . \quad (48)$$

For large and real argument, in the first approximation (with $m' = 0$ and neglecting the remainder in (48)), (46) with $2k_D^2/(\beta_{CD}L) >> 1$ gives

$$e/\langle \in_V^2(L) \rangle^{1/2} \approx (\pi/2)(\beta_{CD}L)^{1/2} , \quad (49)$$

which leads to (44) for the Cauchy limit ($\beta_{CD} = 2es$):

$$e/\langle \in_C^2(L) \rangle^{1/2} = (\pi/2)(2esL)^{1/2} . \quad (50)$$

Because the product Ls is larger than unity even for small L (it was customary to compare RMSS at the arbitrary value of L = 50 Å), the ratio $e/\langle \in_V^2(L) \rangle^{1/2}$ will depend on the strain magnitude. Usually, strain falls in the range 10^{-2}–10^{-3} and it is averaged over a distance comparable to the coherent domain size. Particularly, $\langle D_V \rangle_{v,s}\, s = \langle D_V \rangle_{v,s}/d = N$, the average number of reflecting planes perpendicular to the diffracting vector, is always a large number, and the product Ne is roughly constant and close to unity. A rough estimate from (50) gives a factor of 2 for the strains' ratio. Therefore, it may be concluded that the upper limit of strain e should not differ much from the RMSS in the whole range between the Gauss and Cauchy extremes of the strain-broadened Voigt profile:

$$e/\langle \in_V^2 \rangle^{1/2} = (\pi/2)^{1/2} \approx 1.253 \qquad \text{Gauss strain broadening;} \quad (51)$$

$$0.5 \lesssim e/\langle \in_V^2(L) \rangle^{1/2} \lesssim 2 \qquad \text{otherwise.} \quad (52)$$

Separation of size and strain broadening

From the preceding paragraphs, it is evident that size broadening is angle independent, whereas strain broadening depends on diffracting angle. This is a basis for their separation. Unfortunately, it is immediately obvious from the form of Stokes and Wilson (36) and Warren (37) definition of strain that results will generally disagree. Nowadays, two routes are used mostly: Warren-Averbach method[10] and the integral-breadth methods. Because they use differently defined parameters, the results disagree. However, it will be shown that this limitation can be overcome.

Warren-Averbach method

Because convolutions of size-broadened and strain broadened profiles in real space are calculated simply as products of their respective Fourier transforms, the Fourier coefficients of a physically broadened line profile are the product of size and distortion coefficients:

$$A(L,s) = A_S(L)\, A_D(L,s) \tag{53}$$

where coefficients are given by (18) and (37)

$$A_S(L) = \frac{1}{\langle D \rangle_s} \int_L^\infty (L' - L)\, p_s(L')\, \mathrm{d}L' ; \quad A_D(L,s) = \langle \exp(2\pi i s L \epsilon(L)) \rangle . \tag{54}$$

By taking the approximation (38) for the distortion coefficient, the well-known Warren-Averbach[10] method of separation of size and strain broadening is obtained:

$$\ln A(L,s) = \ln A_S(L) - 2\pi^2 s^2 L^2 \langle \epsilon^2(L) \rangle . \tag{55}$$

They derived this relationship in a different way, by expanding the logarithm of the cosine in power series. It must be noted that, regardless of its derivation, the Warren-Averbach method does not necessarily assume a Gauss strain distribution, or that mean-square strain is independent of distance L. However, the Warren-Averbach approach becomes exact in the case of Gaussian distribution of $\epsilon(L)$ for each L.

Single-Line Methods

There are cases where only the first order of reflection is available or higher-order reflections are severely suppressed (extremely deformed materials, multiphase composites, catalysts, and oriented thin films). Many methods exist to separate size and strain broadening from only one diffraction peak (see review by Delhez, de Keijser, and Mittemeijer[22]). However, because the different size and strain broadening angle dependence is a basis for their separation, the single-line methods should be used only when no other option exists, and very cautiously.

The single-line methods can be divided into two main parts: Fourier-space and real-space methods. All real-space methods are based on the assumption that the Cauchy function determines size and that the Gauss function gives strain. The widely used method of de Keijser *et al.*[71] approximates size and strain parameters from Cauchy and Gauss parts of the Voigt function, respectively:

$$\langle D \rangle_v = \frac{1}{\beta_C} ; \tag{56}$$

$$e = \frac{\beta_G}{2s} . \tag{57}$$

However, the main problem remains that the angle dependence of line broadening is not specified. Some Fourier-space methods might be preferred for dealing with this problem. They are based on the Warren-Averbach separation of size and strain broadening. The functional form of $\langle \epsilon^2(L) \rangle$ is assumed either to be constant, or the more likely behavior to depend on L as $\langle \epsilon^2(L) \rangle = c/L$,[72] which inherently defines the dependence of strain broadening on diffraction angle. All Fourier-space methods, however, have a serious problem that the Fourier coefficients $A(L)$ are usually uncertain for small L, because of the »hook« effect, thus drastically reducing their accuracy.

Simplified multiple-line integral-breadth methods

To separate size and strain broadening by using integral breadths, it is necessary to define the functional form for each effect. Ruland[73] reviewed some analytical functions for modeling both physical and instrumental effects and gave formulas for their convolutions. Schoening[48] suggested the Cauchy size-broadened and Gauss strain-broadened profiles, as well as the modified (power of two) Cauchy function for the strain-broadened profile. The simplest and most used relations are obtained by assuming the Cauchy or Gauss functions for both size-broadened and strain-broadened profiles.[45] Using (17) and (36), with the additive relations for Cauchy and Gauss integral breadths (11) and (12), it follows that

$$\beta = 1/D + 2es ; \tag{58}$$

$$\beta = 1/D + 4e^2 s^2/\beta ; \tag{59}$$

$$\beta^2 = 1/D^2 + 4e^2 s^2 . \tag{60}$$

Equation (58) is often called the Williamson-Hall plot.[74] Equation (59) assumes the Cauchy size-broadened and Gauss strain-broadened profile and uses the Halder and Wagner[49] parabolic approximation (16) for the integral breadth of the Voigt function. These three approximations will be denoted as Cauchy-Cauchy (C-C), Cauchy-Gauss (C-G), and Gauss-Gauss (G-G), respectively.

The G-G assumption is still widely used, although it implies that the physically broadened line profile is a Gauss function, which is highly unlikely, both from the experimental and theoretical points of view. Moreover, it was shown[75] that the G-G approximation may give imaginary domain sizes even in cases where the instrumental function was derived from the suitable standard specimen and the specimen under investigation showed well-resolved reflections. Nowadays, it is accepted that a better approximation to the physically broadened profile is a Voigt function. Particularly, the Cauchy function for the size-broadened and the Gauss function for the strain-broadened profile have both theoretical foundation[2] and widespread use in the single-line methods (see, for instance the review of Delhez, de Keijser and Mittemeijer[22]), meaning that (59) holds. It is also used in many of the Rietveld programs (see Balzar and Ledbetter,[33] Delhez *et al.*,[76] and reviews by Young and Desai,[77] and Le Bail[78]).

From the form of (58)–(60), it is evident that the results will generally disagree but, under special circumstances, they may be equal. Let us consider the case of the first-order and second-order suitably chosen orthorhombic 00*l* reflections (such as pairs 111 and 222, 110 and 220, 002 and 004). With $s_2 = 2s_1$, $r = \beta_2/\beta_1$, $c_1 = 1/\beta_1$, $c_2 = \beta_1/(2s_1)$, (58)–(60) are solved for domain size and strain:

$$D_{C\text{-}C}(r) = c_1 \frac{1}{2-r}; \quad D_{C\text{-}G}(r) = c_1 \frac{4-r}{4-r^2}; \quad D_{G\text{-}G}(r) = 3^{1/2} c_1 \frac{1}{(4-r^2)^{1/2}}; \quad (61)$$

$$e_{C\text{-}C}(r) = c_2(r-1); \quad e_{C\text{-}G}(r) = c_2\left(\frac{r(r-1)}{4-r}\right)^{1/2}; \quad e_{G\text{-}G}(r) = \frac{c_2}{3^{1/2}}(r^2-1)^{1/2}. \quad (62)$$

These equations relate to the formulae of Mitra and Misra.[79] For the »wrongly« assumed Cauchy and Gauss strain distribution, they investigated how domain size and strain depend on the »real« size of domains. Here, we study the behavior of domain size and strain as a function of the ratio of the second-order to the first-order integral breadths r. Figure 7 presents the solutions for $r \geq 1$. The three methods give equal results for the domain size for $r = 1$, $D(1) = 1/\beta_1$, when all the strains are zero, $e(1) = 0$. For $r = 2$, the three methods give equal results for the strain, $e(2) = \beta_1/(2s_1)$, but the domain sizes are infinite. For $r > 2$, $D_{G\text{-}G}$ is not real, whereas both $D_{C\text{-}C}$ and $D_{C\text{-}G}$ are negative. Generally, there are systematic differences in results, being much smaller for strains. Very large differences among the domain size values are obtained as r approaches 2. In the range $1 < r < 2$, the G-G approximation gives the smallest domain size and the largest strain, whereas the C-C approximation does the opposite.

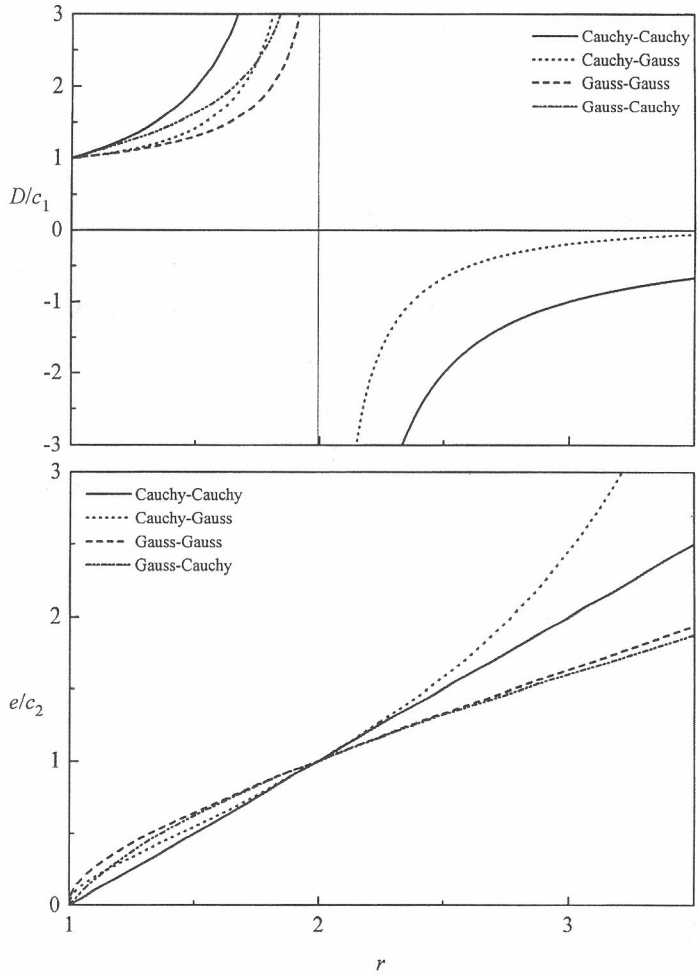

Figure 7. Reduced domain size and strain for four simplified integral-breadth methods as a function of the ratio of the first-order to the second-order integral breadths, r ($r = \beta_2/\beta_1$, $s_2 = 2s_1$, $c_1 = 1/\beta_1$, $c_2 = \beta_1/(2s_1)$.

If Cauchy and Gauss functions are used to model both size-broadened and strain-broadened line profiles, the combination of Gauss size-broadened profile and the Cauchy strain-broadened profile should be investigated, especially in the view of recently reported[23,77,80] line profiles of that type. By using the parabolic approximation in the same way as for (59), the G-C method reads

$$\beta^2 = 1/D^2 + 2es\beta \tag{63}$$

Solutions for domain size and strain, analogous to (61) and (62) are

$$D_{G\text{-}C}(r) = c_1 \left(\frac{2r-1}{r(2-r)} \right)^{1/2} ; \quad e_{G\text{-}C}(r) = c_2 \frac{r^2-1}{2r-1} . \tag{64}$$

For comparison with the other approximations, (64) is plotted in Figure 7. It is obvious that, for $1 < r < 2$, the domain size and strain values are intermediate in relation to the C-C and G-G extremes and similar to the C-G values for both size and strain parameters. This fact emphasizes the inadequacy of all the simplified integral-breadth methods because the actual model (either Cauchy or Gauss function) for the size-broadened or strain-broadened profile becomes irrelevant; they all give comparable results. For $r > 2$, the G-C method behaves much like the G-G approximation because the strain term dominates for large r; domain size is not real while the strain value is the smallest of all obtained by these methods.

Voigt multiple-line integral-breadth methods

In preceding paragraphs, consequences of both size-broadened and strain-broadened Voigt profile were studied. A convolution of two Voigt functions, being a physically broadened profile, is also a Voigt function. The size and strain (distortion) integral breadths of Cauchy and Gauss parts are combined simply:

$$\beta_C = \beta_{CS} + \beta_{CD}(s) ; \tag{65}$$

$$\beta_G^2 = \beta_{GS}^2 + \beta_{GD}^2(s) . \tag{66}$$

This relation assumes that the size component does not depend on s whereas the strain component does depend on s. Data for at least two line profiles are required to solve these equations, contrary to the single-line approaches.

The actual s dependence is determined by the strain model chosen. Currently, two possibilities are used:

(i) Stokes and Wilson[7] definition of »apparent« strain requires that both β_{CD} and β_{GD} be linear functions of s. This approach is built into all simplified integral-breadth methods and introduced in the multiple-line Voigt method by Langford:[81]

$$\beta_C = \beta_{CS} + \beta_{CD} \frac{s}{s_0} ; \tag{67}$$

$$\beta_G^2 = \beta_{GS}^2 + \beta_{GD}^2 \frac{s^2}{s_0^2} . \tag{68}$$

Here, β_{CD}/s_0 and β_{GD}^2/s_0^2 are constant for the pattern and taken conveniently for the first peak.

(ii) Warren[50] definition of mean-square strain requires that the Cauchy and Gauss distortion integral breadths depend differently on s[19] and the same relations read

$$\beta_C = \beta_{CS} + \beta_{CD} \frac{s^2}{s_0^2} ; \tag{69}$$

$$\beta_G^2 = \beta_{GS}^2 + \beta_{GD}^2 \frac{s^2}{s_0^2} . \tag{70}$$

Here, β_{CD}/s_0^2 and β_{GD}^2/s_0^2 are constant for the pattern and »apparent« strain is not independent of diffraction angle because β_{CD} and β_{GD} dependent differently on s. The unknowns β_{CS}, β_{CD}, β_{GS}, and β_{GD} are obtained by plotting both β_C and β_G^2 as functions of s^2 for multiple orders of reflections. This method will be designated as the »double-Voigt« method for brevity, although the Langford's multiple-line Voigt method[81] earlier used the same assumption for size-broadened and strain-broadened integral breadths, that is the Voigt functions.

Both multiple-line Voigt methods will give the simplified integral-breadth methods as limiting cases. However, the results will be different in general because of different definition of strain adopted. Let us consider the »double-Voigt« method only. If the Voigt function approaches either the Cauchy or Gauss extreme in (26) and (40), the relation to the parameters obtained by application of the simplified integral-breadth methods is given in Table V. Both pure-Cauchy and pure-Gauss cases overestimate domain size as compared to the Voigt case for all the values, but especially at extremes of k. Comparing these results with Figure 7, it is clear that, if the strain is present, all the simplified integral-breadth methods overestimate the domain size in relation to the volume-weighted value obtained by the »double-Voigt« method; this being especially valid for the Cauchy-Cauchy assumption. On the contrary, from Table V it seems to follow that the RMSS for both Cauchy and Gauss extremes underestimate the RMSS for the Voigt case. However, we have seen, that strain, although it varies little among different approximations, in a majority of cases will overestimate the RMSS for the Voigt case as well. This complies with the Klug and Alexander[45] discussion and examples from literature on the simplified integral-breadth methods. It was noted[45,82] that the values of domain size scatter much more than the strain among different approximations, including Fourier, vari-

TABLE V

Parameters obtained from the »double-Voigt« method[19] at the Cauchy and Gauss extremes. All symbols explained in text

Parameter	Size broadening			
		k_s	$\langle D_V \rangle_s$	$\langle D_V \rangle_v$
Cauchy (C) extreme	$\beta_{CS} = 0$	∞	$1/(2\beta_{CS})$	$1/\beta_{CS}$
	$\langle D_C \rangle_v / \langle D_V \rangle_v = \exp(-k_S^2) / (\pi^{1/2} k_S \operatorname{erfc}(k_S)) > 1$			
Gauss (G) extreme	$\beta_{CS} = 0$	0	∞	$1/\beta_{GS}$
	$\langle D_G \rangle_v / \langle D_V \rangle_v = \exp(-k_S^2) / \operatorname{erfc}(k_S) \geq 1$			

Parameter	Strain broadening		
		$\langle \epsilon_V^2(L) \rangle^{1/2}$	e
Cauchy (C) extreme	$\beta_{GD} = 0$	$(\beta_{CD} / (\pi^2 s^2 L))^{1/2}$	$\beta_{CD}/(2s)$
	$\langle \epsilon_C^2(L) \rangle / \langle \epsilon_V^2(L) \rangle = (1 + (\pi \beta_{GD}^2 L)/(2\beta_{CD}))^{-1} \leq 1$		
Gauss (G) extreme	$\beta_{CD} = 0$	$\beta_{GD}/(2^{1/2}\pi^{1/2}s)$	$\beta_{GD}/(2s)$
	$\langle \epsilon_G^2(L) \rangle / \langle \epsilon_V^2(L) \rangle = (1 + (2\beta_{CD})/(\pi \beta_{GD}^2 L))^{-1} \leq 1$		

ance, and integral-breadth methods. This was attributed to the sensitivity of Fourier and variance methods to the erroneous background. This analysis shows, however, that large differences in domain size may be inherent to the integral-breadth methods. It may also explain why the G-G approximation is used quite often. For $1 \leq r < 2$ it yields the acceptable values of both the domain size (because the values are the least overestimated) and strain (because they do not vary much among different approximations), as seen from Figure 7. However, this fact does not imply that the pure physically broadened line profile is a Gauss function. On the contrary, especially regarding the behavior of a »more acceptable« C-G assumption, it indicates that all three assumptions are too simple to model broadened diffraction line profiles adequately. The C-G assumption by no means gives better results than the other two approximations. On the contrary, it may give negative domain size, and, on the whole, it yields less accurate results for domain size than the G-G approximation. This comparison is illustrated in the next paragraph; see also Balzar and Popović.[83]

Size-strain analysis of W and MgO

If (69) and (70) are combined with (40) one obtains

$$-(2L\beta_C + \pi L^2\beta_G^2) = -(2L\beta_{CS} + \pi L^2\beta_{GS}^2) - 2\pi^2 s^2 L^2 \langle \epsilon^2(L) \rangle . \quad (71)$$

The first two terms are logarithms of $A(L,s)$ and $A_S(L)$ respectively and the equivalence of the »double-Voigt« with the Warren-Averbach method (55) for identical Fourier coefficients $A(L,s)$ becomes evident.[19] Therefore, instead of tedious graphical analysis of Fourier coefficients, one can directly calculate both surface-weighted and volume-weighted domain size from (26), mean-square strain for each L from (40), and both surface-weighted and volume-weighted column-length distribution functions from (21) and (23). Although the results of Stokes deconvolution and convolution fitting gave quite similar physically broadened profiles of both the W and MgO specimens (see earlier in the text), in practice the differences will appear in the subsequent analyses. Thus, we applied the Warren-Averbach method to the Stokes Fourier-deconvoluted coefficients and »double-Voigt« method to the refined parameters of preset physically broadened Voigt profile to see which parameters are in largest disaccord. Table VI gives a comparison of results for the two methods, along with results obtained by application of simplified integral-breadth methods.

Figure 8 gives a much-discussed plot of $\ln A(L)$ as a function of s^2 for W. It agrees well with results given by McKeehan and Warren.[84]

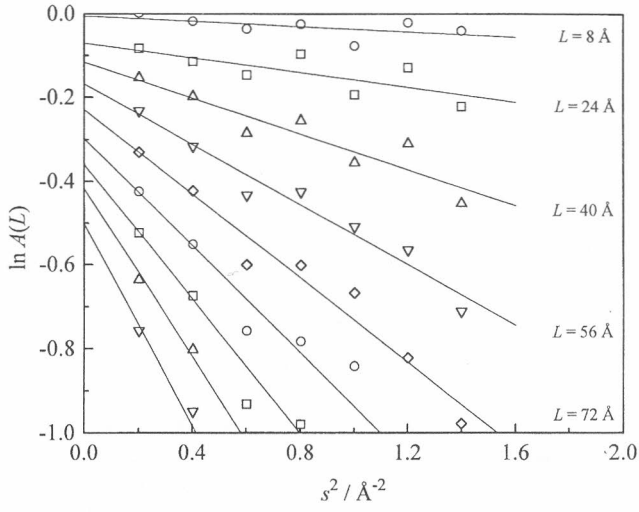

Figure 8. Plot of the first nine odd real Fourier coefficients for seven reflections of W. The ordinate intercepts yield size coefficients and slopes the mean-square strains.

TABLE VI

Comparison of results obtained by application of Warren-Averbach (W-A), the »double-Voigt« (V-V), the multiple-Voigt (M-V) Langford, and simplified integral-breadth methods. The size and strain parameters according to the Cauchy-Cauchy (C-C), Cauchy-Gauss (C-G), and Gauss-Gauss (G-G) methods are calculated from the integral breadths of physically broadened line profiles (columns β (C.F.) from Tables III and IV). All symbols defined in text. Standard uncertainties (s.u.) reflect the random measurement and different fitting errors. They were calculated using the computer program BREADTH[90] according to errors given by Balzar,[91] but for multiple reflections. The s.u. for the simplified methods are similar to those of the »double-Voigt« method but not shown because the likely systematic errors are much larger.

		W	MgO
β_S		2.23	7.84
β_{CS}		2.23	6.47
β_{GS}	$/10^{-3}$ Å^{-1}	imaginary	2.73
β_D		1.66	2.44
β_{CD}		0.334	negative
β_{GD}		1.44	2.44
$\langle D\rangle_s$ (W–A)		340, 209*	79
$\langle D\rangle_s$ (V–V)		224(12)	77(1)
$\langle D\rangle_v$ (V–V)		448(24)	128(1)
$\langle D\rangle_v$ (M–V)	/ Å	870	123
$\langle D\rangle_v$ (C–C)		1883	138
$\langle D\rangle_v$ (C–G)		895	126
$\langle D\rangle_v$ (G–G)		701	125
$\langle\varepsilon^2(a_3)\rangle^{1/2}$ (W–A)		5.10	2.14**
$\langle\varepsilon^2(a_3)\rangle^{1/2}$ (V–V)		4.79(18)	1.45(2)
$\langle\varepsilon^2(\langle D\rangle_s/2)\rangle^{1/2}$ (W–A)		1.53	2.14**
$\langle\varepsilon^2(\langle D\rangle_s/2)\rangle^{1/2}$ (V–V)		1.78(6)	1.45(2)
$\langle\varepsilon^2(\langle D\rangle_v/2)\rangle^{1/2}$ (V–V)	/ 10^{-3}	1.55(6)	1.45(2)
e (M–V)		2.61	1.82
e (C–C)		2.68	0.90
e (C–G)		2.64	1.54
e (G–G)		2.86	2.07

* After the »hook«-effect correction.

** Assumes that strains are approximately independent of L.

The size coefficients, obtained from real Fourier coefficients, are plotted in Figure 9 as a function of distance L. It is interesting to note that they are almost linear, which indicates the Laue size-broadened line profile. This is expected for small crystals, but often approximated with a Cauchy function (see, for instance, Warren[2]). It is seen from Table VI that the size-broadened profile calculated by the »double-Voigt« method is approximately a pure

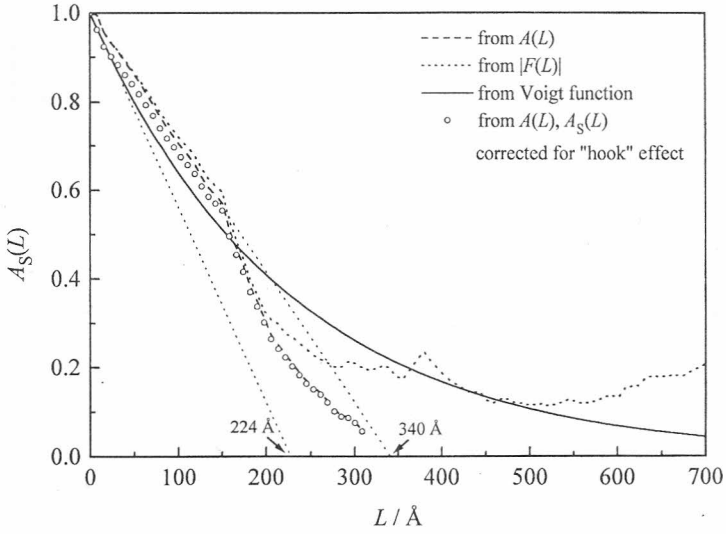

Figure 9. Size coefficients determine the surface-weighted domain size for W which estimates to ~ 224 Å from the »double-Voigt« method and ~ 340 Å from the Warren-Averbach analysis of $A(L)$. After the »hook«-effect correction, the value is closer to that obtained by »double-Voigt« method.

Cauchy function (β^2_{GS} has a small negative value), and a full curve in Figure 9 is an exponential. This is a known case of pure-Cauchy size broadening, which implies $\langle D\rangle_v = 2\langle D\rangle_s$. Domain size determined from the initial slope of $A_S(L)$ is in error because of a small »hook« effect. When corrected, initial Fourier coefficients agree well with the curve obtained from the Voigt function. It is not likely that this »hook« effect originates from the background overestimation, because it would also show through the »double-Voigt« method for background was identical for both cases. Therefore, it may be caused by the uncertainty in a few first Fourier coefficients. Figure 10 shows MSS as a function of distance L. Inherent to the »double-Voigt« analysis, it falls off with $1/L$, whereas MSS calculated by the Warren-Averbach method does not follow it for intermediate and large L, which may be due to uncertainty of Fourier coefficients. In both plots, the same parameters obtained by analyzing of modulus of Fourier coefficients $|F(L)|$ are plotted concurrently.[22] The correspondence of $\langle\epsilon^2(L)\rangle$ (obtained from $A(L)$) and $\langle\epsilon^2(L)\rangle - \langle\epsilon(L)\rangle^2$ (obtained from $|F(L)|$) is a verification that origin and centroid of physically broadened profile coincide. The $A_S(L)$ plot obtained from $|F(L)|$ may look appealing because it seems to follow the full curve up to about 500 Å, but the coefficients are not trustworthy after about 300 Å. It is worthwhile to note that $\beta_S > \beta_D$. That is, contrary to expectation, strain does not appear to be a major source of broadening for ball-milled W. This

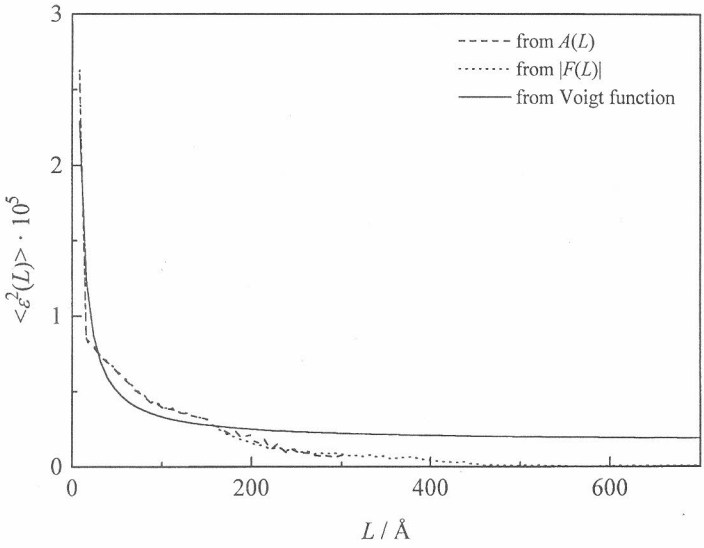

Figure 10. Mean-square strain as a function of averaging distance for the W specimen.

is a good illustration of inadequacy of the simplified integral-breadth methods; they give the opposite impression because both domain sizes and strains are overestimated. In agreement with the observations from the preceding paragraph, the Gauss-Gauss approximation yields the most reliable value of domain size, whereas the Cauchy-Cauchy gives the most reasonable strain, although the differences among strain are much less pronounced. The multiple-line Voigt method[81] gives results much similar to the Cauchy-Gauss approximation in accord with Langford's results.[23] It is interesting to note that the studies of cold-worked W gave very similar results for both domain size and strain, regardless of a mean of deformation: McKeehan and Warren[84] gave values for thoriated-tungsten filings $\langle D\rangle_s$ = 200 Å, $\langle \epsilon^2(\langle D\rangle_s/2)\rangle^{1/2} \approx 2.2 \cdot 10^{-3}$, Aqua and Wagner[85] reported for tungsten filings $\langle D\rangle_s$ = 220 Å, $\langle \epsilon^2(\langle D\rangle_s/2)\rangle^{1/2} \approx 2.7 \cdot 10^{-3}$, Berkum[86] for ball-milled tungsten $\langle D\rangle_s$ = 170 Å, $\langle \epsilon^2(\langle D\rangle_s/2)\rangle^{1/2} \approx 1.3 \cdot 10^{-3}$. Evidently, regardless of type of cold deformation, there is a maximum density and energetically favorable arrangement of dislocations. Only Wagner, Yang, and Boldrick[87] reported as small as $\langle D\rangle_s$ = 35 Å and strain up to $\langle \epsilon^2(\langle D\rangle_s/2)\rangle^{1/2} \approx 6 \cdot 10^{-3}$. This kind of deformation was produced after 20 hours in a high-energy ball mill and explained by the incorporation of Fe and Cr impurities into W particles.

The results for MgO are not less interesting. From the Williamson-Hall plot[74] (Figure 11) it is immediately seen that three reflections can be analyzed simultaneously. Also, the relatively small slope indicates a small strain. Moreover, it is observed that $\beta_C(s)$ has slightly negative slope, mean-

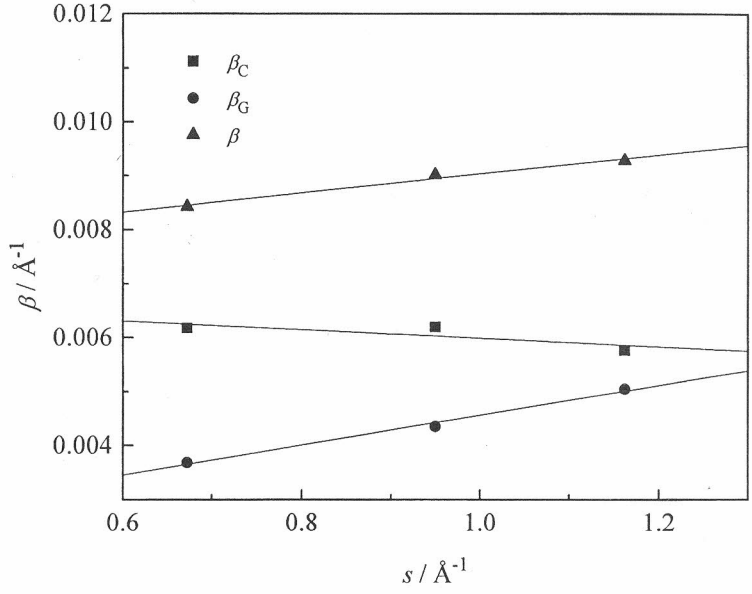

Figure 11. Williamson-Hall plot (Cauchy-Cauchy approximation) for 220, 400, and 422 reflections of MgO.

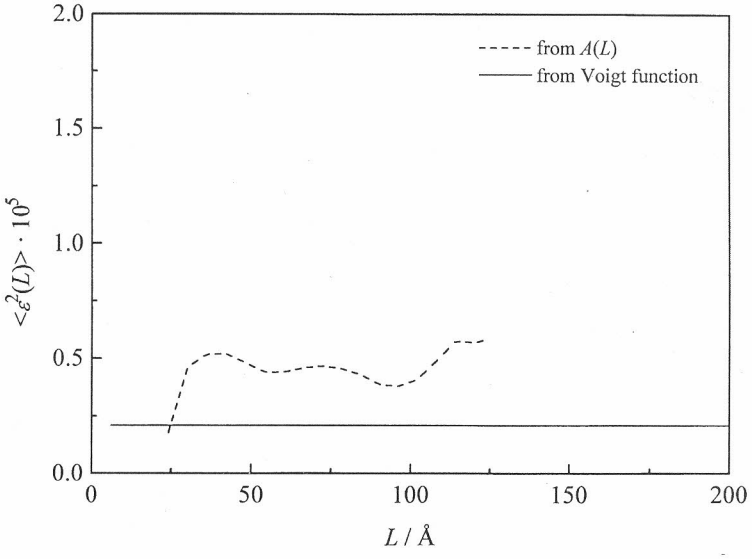

Figure 12. Mean-square strain as a function of averaging distance for the MgO specimen.

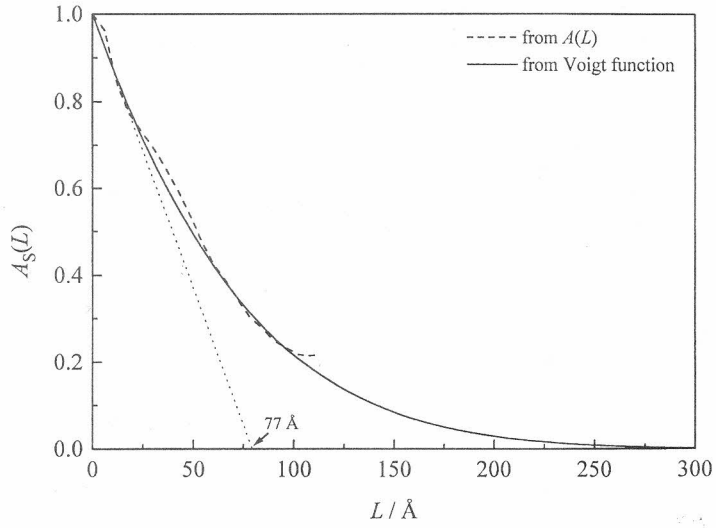

Figure 13. Size coefficients for the MgO specimen.

ing that the strain-broadened profile is a Gauss function. More accurate results are found in Table VI. β_{CD} has a small negative value. In case of pure-Gauss strain broadening, MSS is independent of L and relates to the »maximum« strain e from the integral-breadth methods, according to (51). If the result of »double-Voigt« method is multiplied by 1.253, the strain $1.82 \cdot 10^{-3}$ is obtained, which does fall between C-G and G-G results. Figure 12 shows that Warren-Averbach analysis gives somewhat larger strain. Although values scatter, it is reasonable to assume that it is constant for 30 Å $< L <$ 120 Å. For the first three harmonic numbers, MSS is not real, which is strictly speaking also true for the »double-Voigt« method, because β_{CD} is negative. Although small, this part dominates for smallest L values, according to (40). This behavior was reported for LiF[22] and attributed to the »hook« effect. However, the authors themselves doubted a validity of correcting $A(L)$, instead of $A_S(L)$ (which would not eliminate negative values of MSS). From these results, it is clear that negative values of MSS for smallest L values may be a result of small measurement errors, because at this region MSS change rapidly and are very sensitive to the even small uncertainties in Fourier coefficients. From Figure 13 and Table VI, almost identical results for $\langle D \rangle_s$ follow from the Warren-Averbach and »double-Voigt« methods. Moreover, the values of $\langle D \rangle_v$ concur among all the methods (compare size and strain integral breadths from Table VI) because strain influence on broadening is negligible compared to the size effect, in accordance with previous discussion. It is often assumed, unlike the strain-broadened

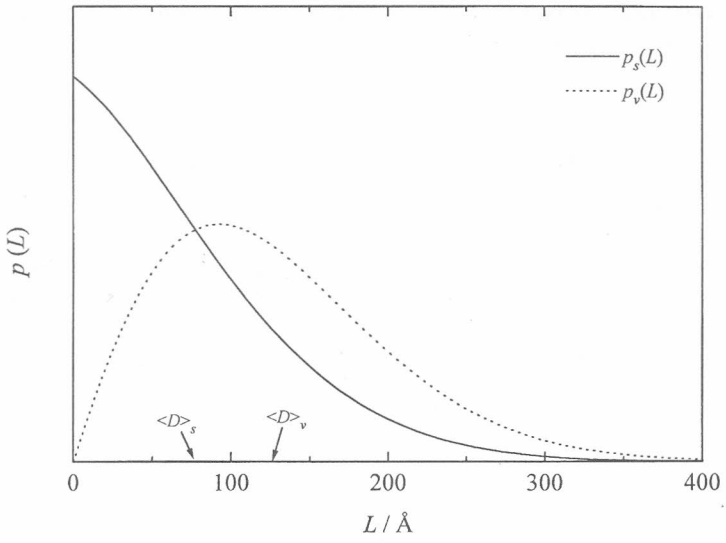

Figure 14. Surface-weighted column-length distribution function, $p_s(L)$, and volume-weighted column-length distribution function, $p_v(L)$, for the MgO specimen.

profile which some authors model with a Voigt function, that a Cauchy function can model the size-broadened profile satisfactorily. Analysis here shows that the (dominant) size broadening in MgO shows a significant Gauss content, which was noted previously.[77] Therefore, a Voigt function as the size-broadened profile seems a better choice.

In principle, it is possible to obtain the column-length distribution function by taking a second derivative of the size coefficients. However, it is clear that there are at least two obstacles: (i) If strain distribution is not exactly Gaussian for every L, the size coefficients are accurate enough only for small harmonic numbers and/or negligible strain; (ii) Even in the case the Gaussian strain distribution can be proven, the high-order size coefficients are unreliable, preventing computation of the column-length distribution function. Few techniques were used to deal with this problem: successive convolution unfolding method,[12] smoothing, and iterative methods.[88,89] The »double-Voigt« method gives a smooth distribution function, as shown in Figure 14. How reliable they are for large L will again depend on the nature of strain distribution. If they agree with Warren-Averbach method for small L, they certainly give more reliable information about true column-length distribution function than the Warren-Averbach method. In case of MgO, strain is rather small. By taking s = 1.16 Å^{-1} for the 422 MgO line and $<\epsilon^2>^{1/2} = 1.45 \cdot 10^{-3}$ from Table VI, the term $2\pi^2 s^2 L^2 <\epsilon^2>$ becomes equal to unity for L = 133.8 Å, that is, about value of $<D>_v$.

McKeehan and Warren[84] have shown that it is possible to derive the strain-distribution functions:

$$p(\epsilon(L)) = 2L \int_0^\infty A_D(L,s) \cos(2\pi sL\epsilon(L))\, ds \,. \tag{72}$$

However, even for eight lines available for W, the $A_D(s)$ curve is not defined adequately and has to be smoothed heavily thus hindering the possible variations. Nevertheless, it is reasonable to assume the Gaussian (or close to it) distribution of strains in general, because all similar bell-shaped distribution functions (Cauchy, Voigt, Pearson VII) yield an infinite mean-square strain

$$\langle \epsilon^2(L) \rangle = \int_{-\infty}^{\infty} \epsilon^2 p(\epsilon(L))\, d\epsilon \,. \tag{73}$$

Surface-weighted domain size and MSS for small values of L are as much reliable information as one can possibly obtain from the Stokes deconvolution and Warren-Averbach analysis in general. In principle, one can calculate the volume-weighted measures of domain size and strain from size and strain integral breadths by taking sums of respective Fourier coefficients:

$$\beta_{f,S,D} = 1 \Big/ \left(a_3 \cdot 2 \sum_{L=0}^{\infty} A_{f,S,D}(L) \right). \tag{74}$$

However, it is difficult to obtain reliable results if the coefficients are not trustworthy.

These two examples showed that, contrary to expectations, it is difficult to treat any case as either size-only or strain-only broadening. MgO does show a prevailing size effect, but the value of strain, as obtained from the Warren-Averbach analysis at $\langle D \rangle_s / 2$, is larger than for W! Also, the size-broadened profile, being a dominant part of physically broadened profile, has a significant Gauss content. The W example shows again that it is unlikely to find a sample with the strain-only broadening. Preparing a specimen without small particles through fractional sedimentation or any other means does not produce a desired effect, because diffraction incoherency exists on the subgrain level.

CONCLUDING REMARKS

Nowadays, diffraction is done using much different tools than decades ago both regarding instrumentation and especially data analysis. Numerous computer programs give solutions for almost any task, and the amount of information obtainable from a simple powder-diffraction scan is astonishing. Hence, it is very likely that the line-broadening analysis will become a part of routine program output, together with the line positions, intensities, lattice parameters, *etc.* The full-pattern-analysis software, such as some Rietveld refinement programs, already includes refinable parameters corresponding to domain size and strain. Unfortunately, inspection of line broadening is rarely a standard procedure. Being so automated, line-broadening analysis is very often inaccurate because of inadequate models used in most Rietveld programs. Instead, the approach based on a Voigt function,[33] generally applicable and likely much more accurate than current models, may be useful.

A frequent objection is that any phenomenological approach with a single analytical function may not correspond to the more realistic model based on physical causes of broadening for a particular specimen. It would be very inconvenient, complicated and maybe even impossible at this moment to build such a specific approach in a Rietveld-refinement program. This is why line shapes in Rietveld programs in the past were not modeled in terms of physically sound parameters. As more and more they are being introduced in the codes, it is wise to find a balance between the accuracy of parameters refined and reasonable universality of a model. Another usual objection to the presumed analytical functions in line-broadening analysis is that data are being »pushed« into the model. Although it is possible to lose useful information by adopting a preset model, this approach should always be weighted against the actually useless information if results are hampered by the inherent errors of some model-independent method.

During decades of research, it became more and more obvious that neither Cauchy nor Gauss functions can adequately model diffraction line broadening. Here it was shown that a model based on a Voigt function may be a more realistic and accurate. Moreover, previously considered as divergent approaches, namely the Warren-Averbach analysis and the integral-breadth methods, are consistently related. Some common occurrences in Warren-Averbach analysis, particularly the »hook« effect, functional dependence of mean-square strain on averaging distance, and ratio of volume-weighted to the surface-weighted domain size, all follow from the »double-Voigt« model. Some possible limitations of Voigt-based models are both of conceptual (asymmetric physically broadened profiles) and practical (observed line profiles may fall bellow of the Voigt Cauchian limit) nature. We may have some better function of choice in the future, but the Voigt function may still prove to be a satisfactory approximation in most cases.

Acknowledgments. – I am most thankful to Dr. Hassel Ledbetter (NIST, Boulder, Colorado) for continuous collaboration and support. Critical comments and suggestions of Professor Stanko Popović (Ruđer Bošković Institute, Zagreb, Croatia) are gratefully acknowledged, as well as the support of the U.S.A. (NIST) – Croatia (Ministry of Science and Technology) Joint Fund (grant No. JF106).

REFERENCES

1. B. E. Warren and B. L. Averbach, *J. Appl. Phys.* **21** (1950) 595–599.
2. B. E. Warren, in *Progress in Metal Physics*, Vol. 8, Pergamon Press, London, 1959, pp. 147–202.
3. M. A. Krivoglaz and K. P. Ryaboshapka, *Phys. Met. Metall.* **15** (1963) 14–26.
4. M. Wilkens, in *Microstructural Characterization of Materials by Non-Microscopical Techniques*, N. H. Andersen, M. Eldrup, N. Hansen, D. J. Jensen, T. Leffers, H. Lilholt, O. B. Pedersen, and B. N. Singh (Eds.), Risø National Laboratory, Roskilde, Denmark, 1984, pp. 153–168.
5. I. Groma, T. Ungár, and M. Wilkens, *J. Appl. Cryst.* **21** (1988) 47–53.
6. P. Scherrer, *Nachr. Gött.* **2** (1918) 98–100.
7. A. R. Stokes and A. J. C. Wilson, *Proc. Phys. Soc. London* **56** (1944) 174–181.
8. A. R. Stokes, *Proc. Phys. Soc. London* **61** (1948) 382–391.
9. E. F. Bertaut, *Acta Cryst.* **3** (1950) 14–18.
10. B. E. Warren and B. L. Averbach, *J. Appl. Phys.* **23** (1952) 497.
11. A. J. C. Wilson, *Nature* **193** (1962) 568–569.
12. S. Ergun, *J. Appl. Cryst.* **1** (1968) 19–23.
13. H. M. Rietveld, *Acta Cryst.* **22** (1967) 151–152.
14. G. S. Pawley, *J. Appl. Cryst.* **14** (1981) 357–361.
15. H. Toraya, *J. Appl. Cryst.* **19** (1986) 440–447.
16. J. I. Langford, *J. Appl. Cryst.* **11** (1978) 10–14.
17. M. Ahtee, L. Unonius, M. Nurmela, and P. Suortti, *J. Appl. Cryst.* **17** (1984) 352–357.
18. R. A. Young and D. B. Wiles, *J. Appl. Cryst.* **15** (1982) 430–438.
19. D. Balzar and H. Ledbetter, *J. Appl. Cryst.* **26** (1993) 97–103.
20. R. Jenkins, in *Modern Powder Diffraction*, Vol. 20, D. L. Bish and J. E. Post (Eds.), The Mineralogical Society of America, Washington, D.C., 1989, pp. 47–71.
21. D. L. Bish and R. C. Reynolds, Jr., in *Modern Powder Diffraction*, Vol. 20, D. L. Bish and J. E. Post (Eds.), The Mineralogical Society of America, Washington, D.C., 1989, pp. 73–99.
22. R. Delhez, Th. H. de Keijser, and E. J. Mittemeijer, *Fresenius Z. Anal. Chem.* **312** (1982) 1–16.
23. J. I. Langford, in *Accuracy in Powder Diffraction II*, NIST Special Publication No. 846, E. Prince and J. K. Stalick (Eds.), National Institute of Standards and Technology, Washington, D.C., 1992, pp. 110–126.
24. D. Louër and J. I. Langford, *J. Appl. Cryst.* **21** (1988) 430–437.
25. D. Taupin, *J. Appl. Cryst.* **6** (1973) 266–273.
26. V. A. Kogan and M. F. Kupriyanov, *J. Appl. Cryst.* **25** (1992) 16–25.
27. R. W. Cheary and A. Coelho, *J. Appl. Cryst.* **25** (1992) 109–121.

28. J. G. M. van Berkum, G. J. M. Sprong, Th. H. de Keijser, R. Delhez, and E. J. Sonneveld, *Powder Diffr.* **10** (1995) 129–139.
29. G. Caglioti, A. Paoletti, and F. P. Ricci, *Nucl. Instrum.* **3** (1958) 223–228.
30. J. I. Langford, *Prog. Cryst. Growth & Charact.* **14** (1987) 185–211.
31. P. Thompson, D. E. Cox, and J. B. Hastings, *J. Appl. Cryst.* **20** (1987) 79–83.
32. J. I. Langford, R. J. Cernik, and D. Louër, *J. Appl. Cryst.* **24** (1991) 913–919.
33. D. Balzar and H. Ledbetter, *Adv. X-ray Anal.* **38** (1995) 397–404.
34. R. Croche and L. Gatineau, *J. Appl. Cryst.* **10** (1977) 479–485.
35. S. A. Howard and K. D. Preston, in *Modern Powder Diffraction,* Vol. 20, D. L. Bish and J. E. Post (Eds.), The Mineralogical Society of America, Washington, D.C., 1989, pp. 217–275.
36. D. Balzar, *J. Appl. Cryst.* **25** (1992) 559–570.
37. W. Kalceff, N. Armstrong, and J. P. Cline, *Adv. X-ray Anal.* **38** (1995) 387–395.
38. S. Twomey, *J. Assoc. Comp. Mach.* **10** (1963) 97–101.
39. J. Skilling and R. K. Bryan, *Mon. Not. R. Astr. Soc.* **211** (1984) 111–124.
40. R. C. Reynolds, in *Modern Powder Diffraction*, Vol. 20, D. L. Bish and J. E. Post (Eds.), The Mineralogical Society of America, Washington, D.C., 1989, pp. 145–182.
41. R. Delhez, Th. H. de Keijser, and E. J. Mittemeijer, in *Accuracy in Powder Diffraction*, NBS Special Publication No. 567, S. Block and C. R. Hubbard (Eds.), National Bureau of Standards, Washington, D.C., 1980, pp. 213–253.
42. L. H. Schwartz and J. B. Cohen, *Diffraction from Materials*, Academic Press, New York, 1977, p. 391.
43. R. Delhez, Th. H. de Keijser, E. J. Mittemeijer, and J. I. Langford, *J. Appl. Cryst.* **19** (1986) 459–466.
44. R. Delhez, Th. H. de Keijser, E. J. Mittemeijer, and J. I. Langford, *Aust. J. Phys.* **41** (1988) 213–227.
45. H. P. Klug and L. E. Alexander, *X-ray Diffraction Procedures*, 2nd edition, John Wiley & Sons, New York, 1974, pp. 618–708.
46. G. K. Wertheim, M. A. Butler, K. W. West, and D. N. E. Buchanan, *Rev. Sci. Instrum.* **11** (1974) 1369–1371.
47. M. M. Hall Jr., V. G. Veeraraghavan, H. Rubin, and P. G. Winchell, *J. Appl. Cryst.* **10** (1977) 66–68.
48. F. R. L. Schoening, *Acta Cryst.* **18** (1965) 975–976.
49. N. C. Halder and C. N. J. Wagner, *Acta Cryst.* **20** (1966) 312–313.
50. B. E. Warren, *X-ray Diffraction*, Addison-Wesley, New York, 1969, pp. 251–314.
51. S. Enzo, G. Fagherazzi, A. Benedetti, and S. Polizzi, *J. Appl. Cryst.* **21** (1988) 536–542.
52. S. A. Howard and R. L. Snyder, *J. Appl. Cryst.* **22** (1989) 238–243.
53. P. Suortti, M. Ahtee, and L. Unonius, *J. Appl. Cryst.* **12** (1979) 365–369.
54. A. Le Bail, *Proc. 10th Colloque Rayons X*, Siemens, Grenoble (1985) 45–59.
55. D. M. A. Guérin, A. G. Alvarez, L. E. Rebollo Neira, A. Plastino, and R. D. Bonetto, *Acta Cryst.* **A42**, 30–35.
56. P. E. Di Nunzio, S. Martelli, and R. R. Bitti, *J. Appl. Cryst.* **28** (1995) 146–159.
57. A. J. C. Wilson, *X-ray Optics*, 2nd edition, Methuen, London, 1962.
58. E. F. Bertaut, *C. R. Acad. Sci.* **228** (1949) 492–494.
59. A. Guinier, *X-ray Diffraction*, W. H. Freeman, San Francisco, 1963.
60. V. N. Selivanov and E. F. Smislov, *Zavod. Lab.* **57** (1991) 28–29.

61. A. P. Prudnikov, Yu. A. Brychkov, and O. I. Marichev, *Integrals and Series*, Vol. 1, Gordon and Breach, Amsterdam, The Netherlands, 1986, p. 344.
62. R. A. Young, R. J. Gerdes, and A. J. C. Wilson, *Acta Cryst.* **22** (1967) 155–162.
63. Th. H. de Keijser, E. J. Mittemeijer, and H. C. F. Rozendaal, *J. Appl. Cryst.* **16** (1983) 309–316.
64. J. I. Langford, R. Delhez, Th. H. de Keijser, and E. J. Mittemeijer, *Aust. J. Phys.* **41** (1988) 173–187.
65. Y. Wang, S. Lee, and Y. Lee, *J. Appl. Cryst.* **15** (1982) 35–38.
66. T. Adler and C. R. Houska, *J. Appl. Phys.* **50** (1979) 3282–3287.
67. C. R. Houska and T. M. Smith, *J. Appl. Phys.* **52** (1981) 748–754.
68. T. Kamiyama, T. Shinohara, S. Tomiyoshi, Y. Minonishi, H. Yamamoto, H. Asano, and N. Watanabe, *J. Appl. Phys.* **68** (1990) 4741–4750.
69. R. L. Rothman and J. B. Cohen, *J. Appl. Phys.* **42** (1971) 971–979.
70. M. Abramowitz and I. A. Stegun (Eds.), *Handbook of Mathematical Functions*, National Bureau of Standards, Washington, D.C., 1964, p. 298.
71. Th. H. de Keijser, J. I. Langford, E. J. Mittemeijer, and B. P. Vogels, *J. Appl. Cryst.* **15** (1982) 308–314.
72. J. Mignot and D. Rondot, *Acta Cryst.* **A33** (1977) 327–333.
73. W. Ruland, *J. Appl. Cryst.* **1** (1968) 90–101.
74. G. K. Williamson and W. H. Hall, *Acta Met.* **1** (1953) 22–31.
75. D. Balzar, H. Ledbetter, and A. Bonefačić, *Mater. Sci. Forum* **166–169** (1994) 79–84.
76. R. Delhez, Th. H. de Keijser, J. I. Langford, D. Louër, E. J. Mittemeijer, and E. J. Sonneveld, in *The Rietveld Method*, R. A. Young (Ed.), Oxford University Press, New York, 1993, pp. 132–166.
77. R. A. Young and P. Desai, *Arch. Nauk Mater.* **10** (1989) 71–90.
78. A. Le Bail, in *Accuracy in Powder Diffraction II*, NIST Special Publication No. 846, E. Prince and J. K. Stalick (Eds.), National Institute of Standards and Technology, Washington, D.C., 1992, pp. 142–153.
79. G. B. Mitra and N. K. Misra, *Brit. J. Appl. Phys. (J. Phys. D)* **1** (1968) 495–499.
80. J. Plévert and D. Louër, *J. Chim. Phys.* **87** (1990) 1427–1440.
81. J. I. Langford, in *Accuracy in Powder Diffraction*, NBS Special Publication No. 567, S. Block and C. R. Hubbard (Eds.), National Bureau of Standards, Washington, D.C., 1980, pp. 255–269.
82. N. C. Halder and C. N. J. Wagner, *Adv. X-ray Anal.* **9** (1966) 91–102.
83. D. Balzar and S. Popović, *J. Appl. Cryst.* **29** (1996) 16–23.
84. M. McKeehan and B. E. Warren, *J. Appl. Phys.* **24** (1953) 52–56.
85. E. N. Aqua and C. N. J. Wagner, *Phil. Mag.* **9** (1964) 565–589.
86. J. G. M. van Berkum, Ph.D. Thesis, Delft University of Technology, Delft, The Netherlands, 1994, p. 173.
87. C. N. J. Wagner, E. Yang, and M. S. Boldrick, *Adv. X-ray Anal.* **35** (1992) 585–592.
88. P. Păuşeşcu, R. Mănăilă, M. Popescu, and E. Jijovici, *J. Appl. Cryst.* **7** (1974) 281–286.
89. A. Le Bail and D. Louër, *J. Appl. Cryst.* **11** (1978) 50–55.
90. D. Balzar, *J. Appl. Cryst.* **28** (1995) 244–245.
91. D. Balzar, *J. Res. Natl. Inst. Stand. Technol.* **98** (1993) 321–353.

SAŽETAK

Proširenje difrakcijske linije – Neprilika ili odraz nesavršenosti kristalne rešetke

Davor Balzar

Difrakcijske linije su proširene iz dva razloga: konfiguracija instrumenta i fizikalni uzroci. Fizikalno širenje daje informaciju o mikrostrukturi materijala. Cijeli postupak analize širenja linija je razmatran, počevši od eksperimentalnog postupka i korekcije za instrumentalno proširenje. U analizi profila proširenog iz fizikalnih razloga, glavnina razmatranja je posvećena široko korištenim metodama odvajanja efekata širenja linija zbog utjecaja veličine domena i deformacije: Warren-Averbach aproksimacija i metode integralne širine. Metode integralne širine su uporedene i razmatrana je njihova pouzdanost. Posebna pažnja je posveæena a priori Voigt funkciji kao modelu za profile proširene zbog veličine domena i deformacije, jer je pokazano da Voigt funkcija zadovoljavajuće aproksimira fizikalne profile linija od W i MgO, koji su dobiveni Stokesovom metodom dekonvolucije. Potonje analize širenja linija su provedene Warren-Averbachovom i »dvostrukom Voigt« metodama i rezultati su upoređeni.

LIST OF SYMBOLS

A, B, C, D	
a, b, c, c_1, c_2,	
m, m'	
U, V, W	
U', V'	General constants
r, z	General variables
A	Fourier coefficient
a_3	Edge of orthorhombic cell, orthogonal to diffracting planes
D	»Apparent« domain size orthogonal to diffracting planes
d	Interplanar spacing
e	»Maximum« (upper limit) strain
FWHM	Full width at half maximum of profile
f, F	Pure-specimen (physically) broadened profile and its Fourier transform
g, G	Instrumentally broadened profile and its Fourier transform
h, H	Observed broadened profile and its Fourier transform
hkl	Miller indices
I	Intensity
K	Scherrer constant
k	$\beta_C/(\pi^{1/2}\beta_G)$, characteristic integral-breadth ratio of a Voigt function
L	na_3, column length (distance between two cells in a real space) orthogonal to diffracting planes
l	Order of reflection
MSS	Mean-square strain
N	Average number of cells per column
n	Harmonic number
p	Column-length distribution function
R	Relative error
RMSS	Root-mean-square strain
s	$2\sin\theta/\lambda = 1/d$, variable in reciprocal space
x	Data-sampling variable: either 2θ or s
β	$\beta(2\theta)\cos\theta_0/\lambda$, integral breadth in units of s ($Å^{-1}$)
γ	Geometrical-aberration profile
$<\epsilon^2(L)>$	Mean-square strain, orthogonal to diffracting planes, averaged over the distance L
η	»Apparent strain«

θ	Diffraction angle
θ_0	Bragg angle of Kα_1 reflection maximum
λ	X-ray wavelength
ω	Wavelength-distribution profile

SUBSCRIPTS

C	Denotes Cauchy (Lorentz) function
D	Denotes distortion-related parameter
f	Denotes physically (pure-specimen) broadened profile
G	Denotes Gauss function
g	Denotes instrumentally broadened profile
h	Denotes observed broadened profile
m	Denotes a maximum index
S	Denotes size-related parameter
s	Denotes surface-weighted parameter
v	Denotes volume-weighted parameter
wp	Denotes weighted-residual error

OPERATORS

$\star$	Convolution: $g(x) \star f(x) = \int g(z)f(x-z)\mathrm{d}z$